

# JULES Technical Documentation

Martin Best

Met Office, Joint Centre for Hydro-Meteorological Research,  
Maclean Building, Crowmarsh Gifford, Wallingford, Oxon. Ox10 8BB, U.K.

This is a combination of the following two documents:  
(with irrelevant parts removed)

MOSES 2.2 technical documentation  
(Hadley Centre Technical Note 30)  
with an update to the surface energy balance for the restructured code

TRIFFID technical documentation  
(Hadley Centre Technical Note 24)

September 29, 2009

# MOSES 2.2 Technical Documentation

Richard Essery, Martin Best and Peter Cox

Hadley Centre, Met Office, London Road, Bracknell, Berks R12 2SY, UK

August 20, 2001

## Abstract

MOSES 2.2 is a new version of the Met Office Surface Exchange Scheme including a tiled representation of heterogeneous surfaces. The implementation of MOSES 2.2 in the radiation, boundary layer and hydrology sections of the Unified Model is described. Instructions are provided for running MOSES 2.2 as a modification to UM version 4.5, as an option in version 5.2 or in an off-line version.

## 1 Introduction

MOSES 2.2 introduces a tiled model of subgrid heterogeneity in the MOSES land-surface scheme. Whereas MOSES 1 (?) used effective parameters to calculate a single surface energy balance for each gridbox, MOSES 2.2 treats subgrid land-cover heterogeneity explicitly. Separate surface temperatures, shortwave and longwave radiative fluxes, sensible and latent heat fluxes, ground heat fluxes, canopy moisture contents, snow masses and snow melt rates are computed for each surface type in a gridbox. Nine surface types are recognized : broadleaf trees, needleleaf trees,  $C_3$  (temperate) grass,  $C_4$  (tropical) grass, shrubs, urban, inland water, bare soil and ice. Except for those classified as land-ice, a land gridbox can be made up from any mixture of the first 8 surface types. Fractions  $\nu_j$  ( $j = 1, \dots, 9$ ) of surface types within each land-surface gridbox are read from an ancillary file or modelled by TRIFFID (?). Air temperature, humidity and windspeed on atmospheric model levels above the surface and soil temperatures and moisture contents below the surface are treated as homogeneous across a gridbox.

Other new features in MOSES 2.2 include :

- Vegetation-dependent surface parameters are calculated on-line from vegetation height and leaf area index rather than read from ancillaries.
- New AVHRR vegetation maps are available.
- An optional spectral albedo scheme calculates separate diffuse and direct beam albedos in visible and near-infrared bands for vegetation tiles, with snow aging parametrized using a prognostic grain size.
- The Penman-Monteith elimination of the surface temperature from the surface energy balance has been extended to include upward longwave radiation, and a diagnostic has been added to output the adjusted TOA outgoing longwave radiation between radiation timesteps.

- Canopy heat capacity and fractional coverage calculations in the optional canopy model have been reformulated.
- An implicit numerical scheme for updating temperatures and moisture contents of soil layers has been introduced.
- An exponential root-depth distribution has been introduced and the conductance for evaporation from bare soil and soil beneath sparse vegetation has been reformulated.
- The code has been restructured as suggested by ? to give a clearer separation between surface and boundary-layer routines. This also bring increments due to snow melt or limited moisture availability within the implicit calculation of surface heat and moisture fluxes.

The performance of MOSES 2.2 is discussed in climate simulations by ? and in mesoscale forecasts by ?.

## 2 Radiation

Rather than the net radiation used in the MOSES I surface energy budget, MOSES 2.2 requires net shortwave radiation on tiles and downward longwave radiation to be calculated by the radiation scheme. Surface albedos are specified either as single values for all bands with diagnosed snow albedos or, if selected by L\_SNOW\_ALBEDO=.TRUE. in namelist NLSTCATM, spectral values with prognostic snow albedos.

### 2.1 All-band albedos

Snow-free and cold deep snow albedos for unvegetated tiles are given in Table 1. Bare soil albedos vary geographically with soil colour, and are read from an ancillary file. For vegetation with leaf area index  $\Lambda$ , snow-free and cold deep snow albedos are

$$\alpha_o = (1 - f_r)\alpha_{\text{soil}} + f_r\alpha_o^\infty, \quad (1)$$

and

$$\alpha_{cds} = (1 - f_r)\alpha_s^o + f_r\alpha_s^\infty, \quad (2)$$

where the radiative fraction,  $f_r$ , is

$$f_r = 1 - e^{-\Lambda/2} \quad (3)$$

and  $\alpha_{\text{soil}}$  is the albedo for snow-free soil underlying the vegetation. Values for the vegetation type dependent parameters  $\alpha_o^\infty$ ,  $\alpha_s^\infty$  and  $\alpha_s^o$  are given in Table 2.

Snow aging is represented by reducing the snow albedo when surface temperature  $T_*$  exceeds  $-2^\circ\text{C}$  according to

$$\alpha_s = \begin{cases} \alpha_{cds} & T_* < T_m - 2 \\ \alpha_{cds} + 0.3(\alpha_o - \alpha_{cds})(T_* - T_m + 2) & T_m - 2 < T_* < T_m \end{cases}, \quad (4)$$

where  $T_m$  is the melting point. For a tile with snow mass  $S$  ( $\text{kg m}^{-2}$ ), the albedo is a weighted average

$$\alpha = \alpha_0 + (\alpha_s - \alpha_0)(1 - e^{-0.2S}). \quad (5)$$

	$\alpha_o$	$\alpha_{c ds}$
Urban	0.18	0.4
Inland water	0.06	0.8
Soil	0.11-0.35*	0.8
Ice	0.75	0.8

Table 1. Snow-free and cold deep snow albedos for unvegetated surface types from NVEGPARM.cdk.

\* Snow-free soil albedos depend on soil colour.

	$\alpha_o^\infty$	$\alpha_s^\infty$	$\alpha_s^o$
Broadleaf trees	0.1	0.15	0.3
Needleleaf trees	0.1	0.15	0.3
C <sub>3</sub> grass	0.2	0.6	0.8
C <sub>4</sub> grass	0.2	0.6	0.8
Shrubs	0.2	0.4	0.8

Table 2. Albedo parameters for vegetation types from PFTPARM.cdk

## 2.2 Spectral albedos

The two-stream canopy radiation model is used for vegetation albedos in the optional spectral albedo scheme. Separate direct-beam and diffuse albedos in visible and near-infrared wave bands are calculated for each vegetation type as

$$\alpha_{\text{dir}} = \frac{h_1}{\sigma} + h_2 + h_3 \quad (6)$$

and

$$\alpha_{\text{dif}} = h_7 + h_8 \quad (7)$$

where

$$h_1 = -dp_4 - cf, \quad (8)$$

$$h_2 = \frac{1}{D_1} \left[ \left( d - \frac{p_3 h_1}{\sigma} \right) (u_1 - h) \frac{1}{S_1} - p_2 S_2 \left( d - c - \frac{h_1}{\sigma} (u_1 + K) \right) \right], \quad (9)$$

$$h_3 = -\frac{1}{D_1} \left[ \left( d - \frac{p_3 h_1}{\sigma} \right) (u_1 + h) S_1 - p_1 S_2 \left( d - c - \frac{h_1}{\sigma} (u_1 + K) \right) \right], \quad (10)$$

$$h_7 = \frac{c}{D_1 S_1} (u_1 - h) \quad (11)$$

and

$$h_8 = -\frac{c S_1}{D_1} (u_1 + h) \quad (12)$$

with

$$\beta_0 = \frac{1 + K}{\omega K} a_s,$$

$$c = \frac{1}{3} (\alpha + \omega),$$

$$\beta = \frac{c}{\omega},$$

$$b = 1 - (1 - \beta)\omega, \quad d = \omega K \beta_0, \quad f = \omega K (1 - \beta_0),$$

$$h = (b^2 - c^2)^{1/2}, \quad \sigma = K^2 + c^2 - b^2,$$

$$u_1 = b - \frac{c}{\alpha_{\text{soil}}},$$

$$S_1 = e^{-h\Lambda}, \quad S_2 = e^{-K\Lambda},$$

$$p_1 = b + h, \quad p_2 = b - h, \quad p_3 = b + K, \quad p_4 = b - K$$

and

$$D_1 = \frac{p_1}{S_1}(u_1 - h) - p_2 S_1(u_1 + h).$$

Assuming a spherical leaf-angle distribution, the single scattering albedo and the optical depth per unit leaf area are

$$a_s = \frac{\omega}{2} \left[ 1 - \mu \ln \left( \frac{\mu + 1}{\mu} \right) \right] \quad (13)$$

and

$$K = \frac{1}{2\mu} \quad (14)$$

for zenith angle cosine  $\mu$ . Parameter values for leaf reflection coefficient  $\alpha$  and leaf scattering coefficient  $\omega$ , which depend on vegetation type and wave band, are given in Table 3.

	$\alpha_{\text{vis}}$	$\alpha_{\text{nir}}$	$\omega_{\text{vis}}$	$\omega_{\text{nir}}$
Broadleaf trees	0.1	0.45	0.15	0.7
Needleleaf trees	0.07	0.35	0.15	0.45
C <sub>3</sub> grass	0.1	0.58	0.15	0.83
C <sub>4</sub> grass	0.1	0.58	0.17	0.83
Shrubs	0.1	0.58	0.15	0.83

Table 3. Spectral albedo parameters from TRIF.cdk.

Snow albedos are calculated using a simplification of the ? parametrization of the ? spectral snow albedo model. The aging of snow is characterized by introducing a prognostic grain size,  $r(t)$ , set to  $r_0 = 50 \mu\text{m}$  for fresh snow and limited to a maximum value of  $2000 \mu\text{m}$ . The change in  $r(t)$  over a timestep  $\Delta t$  is given by

$$r(t + \Delta t) = \left[ r(t)^2 + \frac{G_r}{\pi} \Delta t \right]^{1/2} - [r(t) - r_0] \frac{S_f \Delta t}{d_o}, \quad (15)$$

where  $S_f$  is the snowfall rate during the timestep and  $d_o$ , the mass of fresh snow required to refresh the albedo, is set to  $2.5 \text{ kg m}^{-2}$ . The empirical grain *area* growth rate is

$$G_r = \begin{cases} 0.6 \mu\text{m}^2 \text{ s}^{-1} & T_* = T_m \text{ (melting snow)} \\ 0.06 \mu\text{m}^2 \text{ s}^{-1} & T_* < T_m, r < 150 \mu\text{m} \text{ (cold fresh snow)} \\ A \exp(-E/RT_*) & T_* < T_m, r > 150 \mu\text{m} \text{ (cold aged snow)} \end{cases} \quad (16)$$

where  $A = 0.23 \times 10^6 \mu\text{m}^2 \text{ s}^{-1}$ ,  $E = 37000 \text{ J mol}^{-1}$  and  $R = 8.13451 \text{ J K}^{-1} \text{ mol}^{-1}$ . Snow albedos are calculated as

$$\alpha_{\text{vis}} = 0.98 - 0.002(r^{1/2} - r_0^{1/2}) \quad (17)$$

and

$$\alpha_{\text{nir}} = 0.7 - 0.09 \ln \left( \frac{r}{r_0} \right). \quad (18)$$

The zenith angle dependence is represented by using an effective grain size,

$$r_e = [1 + 0.77(\mu - 0.65)]^2 r, \quad (19)$$

in place of  $r$  in calculations of direct-beam albedos.

For a tile with snow-free albedo  $\alpha_0$ , snowdepth  $d$  and roughness length  $z_0$ , the albedo in each band is

$$\alpha = f_{\text{snow}}\alpha_{\text{snow}} + (1 - f_{\text{snow}})\alpha_0 \quad (20)$$

where

$$f_{\text{snow}} = \frac{d}{d + 10z_0}. \quad (21)$$

## 2.3 Radiation diagnostics

For a gridbox with tile fractions  $\nu_j$ , the gridbox mean albedo

$$\alpha_i = \sum_j \nu_j \alpha_{ij} \quad (22)$$

for band  $i$  and the effective radiative surface temperature

$$T_{*R} = \left( \sum_j \nu_j T_{*j}^4 \right)^{1/4} \quad (23)$$

are used in calculating downward shortwave and longwave radiation fluxes  $LW_{\downarrow}$  and  $SW_{\downarrow i}$ . Surface energy flux calculations require the net all-band shortwave radiation on each tile

$$SW_{Nj} = \sum_i (1 - \alpha_{ij}) SW_{\downarrow i} \quad (24)$$

and

$$\Delta_{\text{OLR}} = \text{OLR} - \sigma T_{*R}^4, \quad (25)$$

which is used in diagnosing the adjustment in TOA outgoing longwave radiation  $\text{OLR}$  due to changes in surface temperature between radiation calls.  $SW_{Nj}$ ,  $LW_{\downarrow}$  and  $\Delta_{\text{OLR}}$  are stored in the RADINCS array for use on timesteps between radiation calls.

## 3 Surface fluxes

### 3.1 Surface roughness and exchange coefficients

Momentum roughness length  $z_o$  is set to  $h/20$  for trees of height  $h$  and  $h/10$  for other vegetation types. Roughness lengths for unvegetated surface types are given in Table 4. The roughness length of a tile with snow mass  $S$  is reduced to  $\max[z_o - 4 \times 10^{-4}S, 5 \times 10^{-4}]$ .

A surface exchange coefficient for sensible and latent heat fluxes between the surface and the lowest atmospheric level at height  $z_1$  over each tile is calculated as  $C_H = f_h C_{Hn}$ , where

$$C_{Hn} = k^2 \left[ \ln \left( \frac{z_1 + z_o}{z_o} \right) \ln \left( \frac{z_1 + z_o}{z_{oh}} \right) \right]^{-1} \quad (26)$$

is the neutral exchange coefficient and

$$f_h = \begin{cases} (1 + 10\text{Ri}_B/\text{Pr})^{-1} & \text{Ri}_B \geq 0 \text{ (stable)} \\ 1 - 10\text{Ri}_B(1 + 10C_{Hn}\sqrt{-\text{Ri}_B}/f_z)^{-1} & \text{Ri}_B < 0 \text{ (unstable)} \end{cases} \quad (27)$$

with scalar roughness length  $z_{oh} = z_o/10$ ,

$$f_z = \frac{1}{4} \left( \frac{z_o}{z_1 + z_o} \right)^{1/2} \quad (28)$$

and Prandtl number

$$\text{Pr} = \ln \left( \frac{z_1 + z_o}{z_o} \right) \left[ \ln \left( \frac{z_1 + z_o}{z_{oh}} \right) \right]^{-1}. \quad (29)$$

The bulk Richardson number is

$$\text{Ri}_B = \frac{gz_1}{U_1^2} \left\{ \frac{1}{T_1} \left[ T_1 - T_* + \frac{g}{c_p} (z_1 + z_{om} - z_{oh}) \right] + \psi \frac{q_1 - q_{\text{sat}}(T_*, p_*)}{q_1 + \epsilon/(1 - \epsilon)} \right\}. \quad (30)$$

for level-1 temperature  $T_1$ , specific humidity  $q_1$  and windspeed  $U_1$ .  $q_{\text{sat}}(T_*, p_*)$  is the saturation humidity at the surface temperature and pressure, and the surface resistance factor  $\psi$  is defined in 3.3. Since  $\psi$  depends on  $C_H$ , routine SF\_RESIST is first called to calculate  $\psi$  assuming neutral conditions, this is passed to routines SF\_RIB and FCDCH for use in calculating  $\text{Ri}_B$  and  $C_H$ , and SF\_RESIST is then called again to calculate a revised value for  $\psi$ .

The above discussion assumes no level-1 cloud and does not include orographic roughness; see Unified Model Documentation Paper 24 (?) for extensions. The alternative formulation of the stability functions used in the new boundary layer scheme is described by Smith and Williams (/home/hc0100/hadaw/public\_html/docs/surf\_exch.ps).

	$z_o$ (m)
Urban	1.5
Water	$3 \times 10^{-4}$
Soil	$3 \times 10^{-4}$
Ice	$1 \times 10^{-4}$

Table 4. Roughness lengths for unvegetated surface types from NVEGPARM.cdk.

### 3.2 Canopy heat capacity

A vegetation canopy model, which introduces a canopy heat capacity and radiative coupling between the canopy and underlying ground, can be selected by editing MOSES\_OPT.cdk to set CAN\_MODEL=3. TRIFFID (?) gives the masses of carbon in leaves and stems per unit area of canopy as  $\sigma_l \Lambda_b$  and  $a_{wl} \Lambda_b^{5/3}$ , where the balanced-growth leaf area index for vegetation of height  $h$  is

$$\Lambda_b = \left( \frac{a_{ws} \eta_{sl} h}{a_{wl}} \right)^{3/2} \quad (31)$$

with parameters given in Table 5. An areal canopy heat capacity,  $C_c$ , is calculated assuming specific heat capacities (in  $\text{kJ K}^{-1}$  per kg of carbon) of 570 for leaves and 110 for wood, based on values given by ? and ?. For non-vegetated tiles, and vegetated tiles if the canopy model is not selected,  $C_c$  is set to zero.

	$a_{wl}$	$a_{ws}$	$\eta_{sl}$	$\sigma_l$
Broadleaf trees	0.65	10	0.01	0.0375
Needleleaf trees	0.65	10	0.01	0.1
C <sub>3</sub> grass	0.005	1	0.01	0.025
C <sub>4</sub> grass	0.005	1	0.01	0.05
Shrubs	0.1	10	0.01	0.05

Table 5. Vegetation parameters from TRIF.cdk.

### 3.3 Evaporation

Surface evaporation is drawn from soil, canopy and snow moisture stores. Evaporation from saturated parts of the surface (lakes, wet vegetation canopies and snow) is calculated at the potential rate (i.e. subject to an aerodynamic resistance only).

Evaporation from transpiring vegetation is controlled by a canopy conductance,  $g_c$ , calculated by a photosynthesis model depending on temperature, humidity deficit, incident radiation, soil moisture availability and vegetation type (?). The ability of vegetation to access moisture at each level in the soil is determined by root density, assumed to follow an exponential distribution with depth. The fraction of roots in soil layer  $k$  extending from depth  $z_{k-1}$  to  $z_k$  is

$$r_k = \frac{e^{-2z_{k-1}/d_r} - e^{-2z_k/d_r}}{1 - e^{-2z_t/d_r}}, \quad (32)$$

where  $d_r$  is the rootdepth for the vegetation type (Table 6) and  $z_t$  is the total depth of the soil model. For transpiration  $E_t$ , the flux extracted from soil layer  $k$  is  $e_k^0 E_t$ , where

$$e_k^0 = \frac{r_k \beta_k}{\sum_k r_k \beta_k} \quad (33)$$

and

$$\beta_k = \begin{cases} 1 & \theta_k \geq \theta_c \\ (\theta_k - \theta_w)/(\theta_c - \theta_w) & \theta_w < \theta_k < \theta_c, \\ 0 & \theta_k \leq \theta_w \end{cases} \quad (34)$$

is a soil moisture availability factor for a soil layer with unfrozen volumetric soil moisture concentration  $\theta_k$ , critical point  $\theta_c$  and wilting point  $\theta_w$ .

Bare-soil evaporation is calculated using a conductivity

$$g_{\text{soil}} = \frac{1}{100} \left( \frac{\theta_1}{\theta_c} \right)^2 \quad (35)$$

and is extracted from the surface soil layer for both bare-soil tiles and fraction  $1 - f_r$  of vegetated tiles (Equation 3). Adding the soil and canopy conductances in parallel to give a total surface conductance  $g_s = g_c + (1 - f_r)g_{\text{soil}}$ , the fraction of the evapotranspiration extracted from each soil layer is

$$e_1 = \frac{g_c e_1^0 + (1 - f_r)g_{\text{soil}}}{g_s} \quad (36)$$

for the surface layer and

$$e_k = \frac{g_c e_k^0}{g_s} \quad (37)$$

for lower layers.

The total evaporation from a tile is  $E = \psi E_0$ , where  $E_0$  is the potential evaporation,

$$\psi = f_a + (1 - f_a) \frac{g_s}{g_s + C_H U_1} \quad (38)$$

and  $f_a$  is the fraction of the tile which is saturated and hence has aerodynamic resistance only;  $f_a = 1$  for lake, ice or snow-covered tiles, and  $f_a = C/C_m$  for a vegetated tile with canopy moisture content  $C$  ( $\text{kg m}^{-2}$ ) and canopy capacity  $C_m = 0.5 + 0.05\Lambda$ . The urban tile is also given a small surface capacity of  $0.5 \text{ kg m}^{-2}$ .

	$d_r$ (m)
Broadleaf trees	3
Needleleaf trees	1
C <sub>3</sub> grass	0.5
C <sub>4</sub> grass	0.5
Shrubs	0.5

Table 6. Rootdepths from PFTPARM.cdk.

### 3.4 Surface energy balance

Surface temperature  $T_*$  is interpreted as a surface skin temperature unless the canopy model is selected, in which case it is a canopy layer temperature for vegetated tiles. In the absence of snowmelt, the surface energy balance for each tile is

$$C_c \frac{dT_*}{dt} = R_N + Q_H - H - LE - G_0, \quad (39)$$

where the surface net radiation is

$$R_N = SW_N + LW_{\downarrow} - \epsilon_c \sigma T_*^4, \quad (40)$$

$Q_H$  is the anthropogenic heat source  $H$  and  $E$  are fluxes of sensible heat and moisture, and  $L$  is the latent heat of vaporization for snow-free tiles or sublimation for snow-covered or ice tiles. The heat flux into the ground, combining radiative (assuming only one reflection) and turbulent fluxes below vegetation canopies and conductive fluxes for the unvegetated fraction, is parametrized as

$$G_0 = f_r [\epsilon_c \epsilon_s (\sigma T_*^4 - \sigma T_s^4) + c_p R K_{Hcan} (T_* - T_s)] + (1 - f_r) \frac{2\lambda}{\Delta z_s} (T_* - T_s) \quad (41)$$

where  $\Delta z_s$  and  $T_s$  are the thickness and temperature of the surface soil layer,  $R K_{Hcan}$  is the turbulent exchange coefficient between the canopy and the underlying soil and  $\epsilon_s$  is the emissivity of the soil. Canopy fraction  $f_r$  is given by Equation (3) if the canopy model is selected but is set to zero otherwise. The thermal conductivity,  $\lambda$ , is equal to the soil conductivity  $\lambda_{soil}$  for snow-free tiles, but is adjusted for insulation by snow of depth  $d$  according to

$$\lambda = \begin{cases} \lambda_{soil} \left[ 1 + \frac{2d}{\Delta z_s} \left( \frac{\lambda_{soil}}{\lambda_{snow}} - 1 \right) \right]^{-1} & d < \Delta z_s / 2 \\ \lambda_{snow} & d \geq \Delta z_s / 2, \end{cases} \quad (42)$$

with  $\lambda_{snow} = 0.265 \text{ W m}^{-1} \text{ K}^{-1}$ .

Expressions for surface fluxes of sensible heat and moisture over each tile are derived from the bulk aerodynamic formulae

$$H = c_p R K_H(1) \left[ T_* - T_1 - \frac{g}{c_p} (z_1 + z_o - z_{oh}) \right] \quad (43)$$

and

$$E = \psi R K_H(1) [q_{sat}(T_*, p_*) - q_1], \quad (44)$$

where  $R K_H(1) = \rho C_H U_1$ ;  $\rho$  and  $c_p$  are the density and heat capacity of air.  $q_{sat}$  can be linearized to give

$$q_{sat}(T_*^{n+1}, p_*) \approx q_{sat}(T_*^n, p_*) + D(T_*^{n+1} - T_*^n), \quad (45)$$

where

$$D = \frac{q_{\text{sat}}(T_*^{(n)}, p_*) - q_{\text{sat}}(T_1^{(n)}, p_*)}{T_*^{(n)} - T_1^{(n)}}. \quad (46)$$

By writing  $T_*^{n+1} = T_*^n + \Delta T_*$ , and linearizing  $(T_*^{n+1})^4$  as

$$(T_*^{n+1})^4 \approx (T_*^n)^4 + 4(T_*^n)^3(T_*^{n+1} - T_*^n) \quad (47)$$

the equations for the turbulent heat and moisture fluxes (equations 43 and 44) and the soil heat flux (equation 41) can be written as

$$H = H_{ex} + c_p R K_H(1) \Delta T_* \quad (48)$$

$$E = E_{ex} + \psi R K_H(1) \Delta T_* \quad (49)$$

$$G_0 = G_{0ex} + [f_r(4\epsilon_c \epsilon_s \sigma (T_*^n)^3 + c_p R K_{Hcan}) + (1 - f_r) \frac{2\lambda}{\Delta z_s}] \Delta T_* \quad (50)$$

where  $H_{ex}$  and  $E_{ex}$  are the explicit heat and moisture fluxes and  $G_{0ex}$  is the explicit soil heat flux. Discretizing the time derivative of  $T_*$  between timesteps  $n$  and  $n + 1$  as

$$\frac{dT_*}{dt} \approx \frac{T_*^{(n+1)} - T_*^{(n)}}{\Delta t}, \quad (51)$$

and using equations (39), (48), (49) and (50) to obtain an expression for  $T_*$  gives

$$\Delta T_* = \frac{R_N^n + Q_H - H_{ex} - E_{ex} - G_{0ex}}{R K_H(1)(c_p + LD\psi) + A'_s} \quad (52)$$

where  $R_N^n = SW_N + LW \downarrow - \epsilon_c \sigma (T_*^n)^4$  is the explicit net radiation and

$$A'_s = 4(1 + \epsilon_s f_r) \epsilon_c \sigma (T_*^n)^3 + f_r c_p R K_{Hcan} + (1 - f_r) \frac{2\lambda}{\Delta z_s} + \frac{C_c}{\Delta t} \quad (53)$$

The value of the surface temperature from equation (52) can then be used in equations (48), (49) and (50) to obtain fluxes that are consistent with the Penman-Monteith equations.

### 3.5 Implicit boundary layer fluxes (1)

Increments in temperatures on boundary-layer levels  $k = 1, \dots, N$  are calculated as

$$\delta T_k = \frac{g \Delta t}{\Delta p_k} [F_T(k+1) - F_T(k)], \quad (54)$$

where the fluxes are

$$F_T(k) = -R K_H(k) \left[ \frac{T_k - T_{k-1}}{\Delta z_{k-1/2}} + \frac{g}{c_p} \right] \quad (55)$$

for  $1 < k \leq N$  with boundary conditions  $F_T(N+1) = 0$  and  $F_T(1) = \bar{H}/c_p$  for gridbox-mean surface sensible heat flux

$$\bar{H} = \sum_j \nu_j H_j. \quad (56)$$

Implicit fluxes during timestep  $n$  are calculated using

$$T_k = (1 - \gamma_k) T_k^{(n)} + \gamma_k T_k^{(n+1)} \quad (57)$$

$$= T_k^{(n)} + \gamma_k \delta T_k \quad (58)$$

where  $\gamma_k$  is the forward timestep weighting factor for level  $k$ . This gives a tridiagonal system of equations

$$\begin{aligned} B_{TN}\delta T_N + C_{TN}\delta T_{N-1} &= (\delta T_N)_{\text{ex}} \\ A_{Tk}\delta T_{k+1} + B_{Tk}\delta T_k + C_{Tk}\delta T_{k-1} &= (\delta T_k)_{\text{ex}} \quad k = 2, \dots, N-1 \\ A_{T1}\delta T_2 + B_{T1}\delta T_1 &= (\delta T_1)_{\text{ex}} - (g\Delta t/\Delta p_1)F_T(1) \end{aligned} \quad (59)$$

with matrix elements

$$A_{Tk} = \gamma_{k+1} \frac{g\Delta t}{\Delta p_k} \frac{RK_H(k+1)}{\Delta z_{k+1/2}} \quad k = 1, \dots, N-1 \quad (60)$$

$$B_{Tk} = \begin{cases} 1 - C_{TN} & k = N \\ 1 - A_{Tk} - C_{Tk} & k = 2, \dots, N-1 \\ 1 - A_{T1} & k = 1 \end{cases} \quad (61)$$

and

$$C_{Tk} = \gamma_k \frac{g\Delta t}{\Delta p_k} \frac{RK_H(k)}{\Delta z_{k-1/2}} \quad k = 2, \dots, N. \quad (62)$$

The explicit increments on the rhs of Equation (59) are

$$(\delta T_k)_{\text{ex}} = \begin{cases} -(g\Delta t/\Delta p_N)F_T^{(n)}(N) & k = N \\ (g\Delta t/\Delta p_N)[F_T^{(n)}(k+1) - F_T^{(n)}(k)] & k = 2, \dots, N-1 \\ (g\Delta t/\Delta p_1)F_T^{(n)}(2) & k = 1 \end{cases} \quad (63)$$

where the explicit fluxes are given by Equation (55) with temperatures at the beginning of the timestep. A downward sweep to eliminate the below-diagonal elements in (59) gives

$$\begin{aligned} \delta T_k + C'_{Tk}\delta T_{k-1} &= \delta T'_k \quad k = 2, \dots, N \\ \delta T_1 &= \delta T'_1 - \beta F_T(1) \end{aligned} \quad (64)$$

where  $C'_{Tk} = C_{Tk}/B'_{Tk}$  with

$$B'_{Tk} = \begin{cases} 1 - C_{TN} & k = N \\ 1 - A_{Tk}(1 + C'_{Tk+1}) - C_{Tk} & k = 2, \dots, N-1 \\ 1 - A_{T1}(1 + C'_{T2}) & k = 1 \end{cases} \quad (65)$$

$$\beta = \frac{g\Delta t}{\Delta p_k} \frac{1}{B'_{Tk}} \quad (66)$$

and

$$\delta T'_k = \begin{cases} (\delta T_N)_{\text{ex}}/B'_{TN} & k = N \\ [(\delta T_k)_{\text{ex}} - A_{Tk}\delta T'_{k+1}]/B'_{Tk} & k = 1, \dots, N-1 \end{cases} \quad (67)$$

An analogous set of equations links the humidity increments and the gridbox-mean surface evaporation.

### 3.6 Implicit surface fluxes

Writing the level-1 temperature and humidity as

$$T_1 = T_1^{(n)} + \gamma_1 \delta T_1 \quad (68)$$

and

$$Q_1 = Q_1^{(n)} + \gamma_1 \delta Q_1 \quad (69)$$

in Equations (43) and (44), taking gridbox means gives

$$\frac{\overline{H}}{c_p} = \sum_j \nu_j \frac{H_j^{(n)}}{c_p} + A_1 \delta T_1 + A_2 \delta Q_1 \quad (70)$$

and

$$\overline{E} = \sum_j \nu_j E_j^{(n)} + B_1 \delta T_1 + B_2 \delta Q_1, \quad (71)$$

where

$$A_1 = -\gamma_1 \sum_j \nu_j RK_{PMj} [LD_j \psi_j RK_H(1)_j + A_{*j}], \quad (72)$$

$$A_2 = \gamma_1 \sum_j \nu_j RK_{PMj} L \psi_j RK_H(1)_j, \quad (73)$$

$$B_1 = \gamma_1 c_p \sum_j \nu_j RK_{PMj} D_j \psi_j RK_H(1)_j \quad (74)$$

and

$$B_2 = -\gamma_1 \sum_j \nu_j RK_{PMj} \psi_j [c_p RK_H(1)_j + A_{*j}]. \quad (75)$$

Substituting Equation (64) for  $\delta T_1$  and the analogous equation for  $\delta Q_1$  in Equations (70) and (71), solving for the gridbox-mean fluxes gives

$$\frac{\overline{H}}{c_p} = \frac{(1 + \beta B_2)[F_T(1)^{(n)} + A_1 \delta T'_1 + A_2 \delta Q'_1] - \beta A_2 [F_Q(1)^{(n)} + B_1 \delta T'_1 + B_2 \delta Q'_1]}{(1 + \beta A_1)(1 + \beta B_2) - \beta^2 A_2 B_1} \quad (76)$$

and

$$\overline{E} = \frac{(1 + \beta A_1)[F_Q(1)^{(n)} + B_1 \delta T'_1 + B_2 \delta Q'_1] - \beta B_1 [F_T(1)^{(n)} + A_1 \delta T'_1 + A_2 \delta Q'_1]}{(1 + \beta A_1)(1 + \beta B_2) - \beta^2 A_2 B_1}. \quad (77)$$

Tile fluxes are recovered as

$$\frac{H_j}{c_p} = \frac{H_j^{(n)}}{c_p} - \gamma_1 RK_{PMj} [LD_j \psi_j RK_H(1)_j + A_{*j}] [\delta T'_1 - \beta \overline{H} / c_p] \quad (78)$$

$$+ \gamma_1 RK_{PMj} L \psi_j RK_H(1)_j [\delta Q'_1 - \beta \overline{E}] \quad (79)$$

and

$$E_j = E_j^{(n)} + \gamma_1 RK_{PMj} D_j \psi_j RK_H(1)_j [c_p \delta T'_1 - \beta \overline{H}] \quad (80)$$

$$- \gamma_1 RK_{PMj} \psi_j [c_p RK_H(1)_j + A_{*j}] [\delta Q'_1 - \beta \overline{E}]. \quad (81)$$

A first estimate of the surface temperature for each tile is diagnosed as

$$T_* = T_s + \frac{1}{A_*} \left[ R_s - H - LE + \frac{C_c}{\Delta t} (T_*^{(n)} - T_s) \right]. \quad (82)$$

This has to be adjusted if evaporation exhausts any of the moisture stores during the timestep or if the tile has a melting snowcover.

### 3.6.1 Limited evaporation

Downward surface moisture fluxes are added to canopy moisture or, if the surface temperature is below freezing, snowcover.

For an upward total moisture flux  $E$ , the rates of evaporation from the canopy and soil moisture stores are

$$E_c = f_a \frac{E}{\psi} \quad (83)$$

and

$$E_s = (1 - f_a) \psi_s \frac{E}{\psi} \quad (84)$$

where

$$\psi_s = \frac{g_s}{g_s + C_H U_1}. \quad (85)$$

If the predicted canopy evaporation would exhaust the canopy moisture store  $C$  during a timestep, the soil evaporation is recalculated as

$$E_s = \psi_s \left( 1 - \frac{f_a C}{E_c \Delta t} \right) \frac{E}{\psi} \quad (86)$$

and  $E_c$  is reset to  $C/\Delta t$  (see ?). If  $E_s$  would then exhaust the available soil moisture  $m$ , it is limited to  $m/\Delta t$ .

For an adjustment  $\Delta(LE)$  in the latent heat flux, repartitioning the surface energy balance gives adjustments

$$\Delta H = - \left[ 1 + \frac{A_*}{c_p R K_H(1)} \right]^{-1} \Delta(LE) \quad (87)$$

and

$$\Delta T_* = - \frac{\Delta H + \Delta(LE)}{A_*} \quad (88)$$

in the surface sensible heat flux and temperature.

Evaporation from a lake tile (or the lake fraction of an aggregated surface) is not limited and does not draw on the conserved moisture stores.

### 3.6.2 Snowmelt

Equation (39) neglects snowmelt heat fluxes in the surface energy balance. If  $T_* > T_m$  for a snow-covered tile and sufficient snow is available,  $T_*$  is reset to  $T_m$  by adding an increment

$$\Delta T_* = T_m - T_*, \quad (89)$$

corresponding to a snowmelt heat flux

$$S_m = -[(c_p + L_s D) R K_H(1) + A_*] \frac{\Delta T_*}{L_f}. \quad (90)$$

The maximum melt rate that can be sustained over a timestep  $\Delta t$ , however, is  $S/\Delta t - E$ , giving

$$\Delta T_* = \frac{L_f (S/\Delta t - E)}{(c_p + L_c D) R K_H(1) + A_*}. \quad (91)$$

$\Delta T_*$  is set to the smaller of the values given by Equations (90) and (91), and the surface energy balance is repartitioned by adding increments

$$\Delta H = c_p R K_H(1) \Delta T_* \quad (92)$$

and

$$\Delta E = D R K_H(1) \Delta T_* \quad (93)$$

to the tile heat and moisture fluxes.

### 3.7 Implicit boundary layer fluxes (2)

After adjustment of the surface fluxes, an upward sweep through the matrix equation gives temperature increments

$$\delta T_1 = \delta T'_1 - \beta \overline{H} / c_p, \quad (94)$$

$$\delta T_k = \delta T'_k - C'_{T_k} \delta T_{k-1} \quad k = 2, \dots, N \quad (95)$$

and humidity increments

$$\delta Q_1 = \delta Q'_1 - \beta \overline{E}, \quad (96)$$

$$\delta Q_k = \delta Q'_k - C'_{T_k} \delta Q_{k-1} \quad k = 2, \dots, N. \quad (97)$$

### 3.8 Screen level diagnostics

Screen level exchange coefficients are calculated for each tile by the same interpolation method as currently used by the boundary-layer scheme in routine SFL\_INT. Air temperatures and humidities over tiles are calculated by SCREEN\_TQ and averaged to give gridbox-mean values, which are converted from cloud-conserved forms to actual temperatures and humidities by BL\_CTL. This conversion is required if level-1 cloud is present, but has not been applied to the individual tile diagnostics.

## 4 Hydrology

### 4.1 Surface hydrology

The partitioning of precipitation into interception, throughfall, runoff and infiltration is the same as described in UM Documentation Paper 25 (?) but is applied separately on each tile. For rainfall rate  $R$  covering fraction  $\epsilon$  of a gridbox (1 for large-scale rain or condensation and 0.3 for convective rain), the throughfall from the canopy on a vegetated tile is calculated as

$$T_F = R \left( 1 - \frac{C}{C_m} \right) \exp \left( -\frac{\epsilon C_m}{R \Delta t} \right) + R \frac{C}{C_m} \quad (98)$$

and the tile canopy water content is updated by

$$C^{(n+1)} = C^{(n)} + (R - T_F) \Delta t. \quad (99)$$

Surface runoff is calculated as

$$Y = \begin{cases} R \frac{C}{C_m} \exp \left( -\frac{\epsilon K C_m}{R C} \right) + R \left( 1 - \frac{C}{C_m} \right) \exp \left( -\frac{\epsilon C_m}{R \Delta t} \right) & K \Delta t \leq C \\ R \exp \left[ -\frac{\epsilon (K \Delta t + C_m - C)}{R \Delta t} \right] & K \Delta t > C \end{cases} \quad (100)$$

where the surface infiltration rate  $K$  is equal to  $\beta K_s$ ;  $K_s$  is the soil saturated hydrological conductivity and  $\beta$  is an enhancement factor, values of which are given in Table 7. Runoff of melt water is calculated using snowmelt rate  $S_m$  in place of  $R$  and  $\epsilon = 1$ . The flux of water into the soil is given by the gridbox average

$$W_0 = \sum_j \nu_j (T_{Fj} + S_{mj} - Y_j). \quad (101)$$

	$\beta$		$\beta$
Broadleaf trees	4	Urban	0.1
Needleleaf trees	4	Water	0
C <sub>3</sub> grass	2	Soil	0.5
C <sub>4</sub> grass	2	Ice	0
Shrubs	2		

Table 7. Infiltration enhancement factors from PFTPARM.cdk and NVEGPARM.cdk.

## 4.2 Soil Thermodynamics

As in MOSES I, subsurface temperatures are updated using a discretized form of the heat diffusion equation, which is coupled to the soil hydrology module through:

- soil water phase changes and the associated latent heat
- soil thermal characteristics which are dependent on soil moisture content (liquid water and ice).

The temperature of the  $n^{\text{th}}$  soil layer, of thickness  $\Delta z_n$ , is incremented by the diffusive heat fluxes into and out of the layer,  $G_{n-1}$  and  $G_n$  respectively, and the net heat flux,  $J_n$ , advected from the layer by the moisture flux:

$$C_A \Delta z_n \frac{dT_n}{dt} = G_{n-1} - G_n - J_n \Delta z_n \quad (102)$$

The diffusive and advective fluxes are given by:

$$G = \lambda \frac{\partial T}{\partial z} \quad (103)$$

$$J = c_w W \frac{\partial T}{\partial z} \quad (104)$$

where  $z$  is the vertical coordinate,  $W$  is the vertical flux of soil moisture (calculated within the soil hydrology module),  $c_w$  is the specific heat capacity of water, and  $\lambda$  is the local soil thermal conductivity (?), modified in the presence of lying snow (see 3.4). The ‘‘apparent’’ volumetric heat capacity of the layer,  $C_A$ , is given by:

$$C_A = C_s + \rho_w c_w \Theta_u + \rho_i c_i \Theta_f + \rho_w \{ (c_w - c_i) T + L_f \} \frac{\partial \Theta_u}{\partial T} \quad (105)$$

where  $\Theta_u$  and  $\Theta_f$  are the volumetric concentrations of frozen and unfrozen soil moisture, and  $\rho_i$  and  $c_i$  are the density and specific heat capacity of ice. The first three terms on the right hand side of Equation (105) represent contributions from dry soil, liquid water and ice, and the final term is the apparent heat capacity associated with phase changes. The relationship between unfrozen water concentration,  $\Theta_u$ , and temperature,  $T$ , can be derived by minimizing the Gibbs free energy

of the soil-water-ice system (?). This results in an equation relating the water suction,  $\Psi$  (m), to the temperature,  $T$  (K), when ice is present (?):

$$\Psi = -k \left\{ \frac{\rho_i L_f}{\rho_w T_m g} \right\} (T - T_m) \quad (106)$$

where  $T_m$  (K) is the freezing point of pure water,  $g$  is the acceleration due to gravity and  $k$  is a dimensionless constant which depends on the nature of the soil. A value of  $k = 1.0$  is assumed, which is consistent with a clay-rich soil for which absorption forces dominate over capillary forces. ( $k = 2.2$  would be more appropriate for granular soils (?)). Combining Equation (106) with the ? form (Equation 119) for the suction as a function of liquid water yields:

$$\frac{\Theta_u^{max}}{\Theta_s} = \left\{ -\frac{\kappa(T - T_m)}{\Psi_s} \right\}^{-1/b} \quad (107)$$

where  $\Theta_u^{max}$  is the maximum unfrozen water that can exist at temperature  $T$ ,  $\Theta_s$  is the saturation soil moisture concentration,  $\Psi_s$  and  $b$  are other soil specific parameters and  $\kappa$  is a constant defined by:

$$\kappa = k \frac{\rho_i L_f}{\rho_w g T_m} \approx 114.3 \text{ m K}^{-1} \quad (108)$$

The actual value of  $\Theta_u$  is limited by the total water content of the soil:

$$\Theta_u = \min \{ \Theta_u^{max}, \Theta \} \quad (109)$$

where  $\Theta$  is the “liquid” total volumetric concentration, i.e. that which would arise if all the moisture was in liquid form:

$$\Theta = \Theta_u + \frac{\rho_i}{\rho_w} \Theta_f \quad (110)$$

The temperature above which all soil moisture is unfrozen,  $T_{max}$ , can be derived by equating  $\Theta$  to  $\Theta_u^{max}$  in Equation (107):

$$T_{max} = T_m - \frac{\Psi_s}{\kappa} \left\{ \frac{\Theta_s}{\Theta} \right\}^b \quad (111)$$

The second term on the right hand side represents the suppression of the initial freezing point. It is useful to rewrite Equation (109) in terms of two distinct temperature regimes:

$$\Theta_u = \begin{cases} \Theta_u^{max} & \text{if } T < T_{max} \\ \Theta & \text{if } T \geq T_{max} \end{cases} \quad (112)$$

then differentiation with respect to temperature yields:

$$\frac{\partial \Theta_u}{\partial T} = \begin{cases} \frac{\kappa \Theta_s}{b \Psi_s} \left\{ -\frac{\kappa(T - T_m)}{\Psi_s} \right\}^{(-1/b-1)} & \text{if } T < T_{max} \\ 0 & \text{if } T > T_{max} \end{cases} \quad (113)$$

which is used in Equation (105). The surface soil heat flux,  $G_0$ , is calculated in boundary layer routine SF\_IMPL as a residual in Equation (39). Heat advection by surface infiltration is currently neglected. The lower boundary condition corresponds to zero vertical gradient in soil temperature.

### 4.3 Soil Hydrology

The soil hydrology component of MOSES 2.2 is based on a finite difference approximation to the Richards' equation (?), with the same vertical discretization as the soil thermodynamics module. The prognostic variables of the model are the total soil moisture content within each layer:

$$M = \rho_w \Delta z \Theta_s \{S_u + S_f\} \quad (114)$$

where  $\Delta z$  is the thickness of the layer, and  $S_u$  and  $S_f$  are the mass of unfrozen and frozen water within the layer as a fraction of that of liquid water at saturation:

$$S_u = \frac{\Theta_u}{\Theta_s} \quad (115)$$

$$S_f = \frac{\rho_i}{\rho_w} \frac{\Theta_f}{\Theta_s} \quad (116)$$

The total soil moisture content within the  $n^{\text{th}}$  soil layer is incremented by the diffusive water flux flowing in from the layer above,  $W_{n-1}$ , the diffusive flux flowing out to the layer below,  $W_n$ , and the evapotranspiration extracted directly from the layer by plant roots and soil evaporation,  $E_n$ :

$$\frac{dM_n}{dt} = W_{n-1} - W_n - E_n \quad (117)$$

$E_n$  is calculated from the total evapotranspiration,  $E_t$ , based on the profiles of soil moisture and root density,  $E_n = e_n E_t$ . The  $e_n$  weighting factors are described in section 3.3. The water fluxes are given by the Darcy equation:

$$W = K \left\{ \frac{\partial \Psi}{\partial z} + 1 \right\} \quad (118)$$

where  $K$  is the hydraulic conductivity and  $\Psi$  is the soil water suction. To close the model it is necessary to assume forms for the hydraulic conductivity and the soil water suction as a function of the soil moisture concentration. The dependencies suggested by ? are most often used in GCM land-surface schemes, primarily because of their relative simplicity. In addition the work of ? offers a means of linking the parameters which define these curves to soil particle size distribution. More sophisticated dependencies, such as those derived by ?, can be included with fairly minor code modification. However, the Clapp and Hornberger relations are currently used by default in MOSES 2:

$$\Psi = \Psi_s S_u^{-b} \quad (119)$$

$$K = K_s S_u^{2b+3} \quad (120)$$

where  $K_s$ ,  $\Psi_s$  and  $b$  are empirical soil dependent constants. The interpretation of the Clapp-Hornberger relations in terms of unfrozen rather than total soil moisture is consistent with the observation that the freezing of soil moisture reduces hydraulic conductivity and produces a large suction by reducing the unfrozen water content (?).

The top boundary condition for the soil hydrology module is given by Equation (101). The default lower boundary condition corresponds to "free drainage":

$$W_N = K_N \quad (121)$$

where  $W_N$  is the drainage from the lowest deepest soil layer and  $K_N$  is the hydraulic conductivity of this layer.

## 4.4 Soil numerics

A key difference between the MOSES I soil scheme and that used in MOSES 2.2 concerns the numerical scheme used to update soil moisture and soil temperatures through Equations (102) and (117). MOSES I used a simple explicit scheme, in which the fluxes on the righthandside of these equations are calculated from the beginning of timestep values of  $T$  and  $M$ . By contrast, MOSES 2.2 includes an implicit scheme which remains numerically stable and accurate at much longer timesteps and higher vertical resolution. Although this scheme has a relatively small impact on the model performance at the standard soil model resolution (4 soil layers with thicknesses from the top of 0.1, 0.25, 0.65, 2.0 metres), it does make it feasible for users to choose many more soil layers without incurring massive computational costs (see for example ?).

The prognostic equations for the soil (Equations 102 and 117) take the form:

$$\frac{dY_n}{dt} = F_{n-1} - F_n - s_n \quad (122)$$

where  $Y_n = \{T_n, M_n\}$ ,  $F_n = \{G_n/C_A, W_n\}$  and  $s_n = \{J_n/C_A, E_n\}$ . The fluxes  $F_n$  are a function of the prognostic variables  $Y_n$ . In the explicit MOSES I scheme the  $F_n$  were calculated using the values of  $Y_n$  at the beginning of timestep  $t$ , denoted  $Y_n^t$ . In MOSES 2.2 these same fluxes are calculated using a forward timestep weighting,  $\gamma$ , such that:

$$F_n = F_n^t + \gamma \frac{\partial F_n}{\partial Y_n} \Delta Y_n + \gamma \frac{\partial F_n}{\partial Y_{n+1}} \Delta Y_{n+1} \quad (123)$$

where  $\Delta Y_n$  is the increment to  $Y_n$  during the timestep  $t$  to  $t + \Delta t$ . The derivatives of the fluxes with respect to the prognostic variables are calculated in subroutines DARCY, HYD\_CON and SOIL\_HTC. Equation (123) can be substituted into Equation (122) to yield a series of  $n$  simultaneous equations for the  $n$  prognostic variables:

$$a_n \Delta Y_{n-1} + b_n \Delta Y_n + c_n \Delta Y_{n+1} = d_n \quad (124)$$

where:

$$\begin{aligned} a_n &= -\gamma \Delta t \frac{\partial F_{n-1}}{\partial Y_{n-1}} \\ b_n &= \Delta z - \gamma \Delta t \left[ \frac{\partial F_{n-1}}{\partial Y_n} - \frac{\partial F_n}{\partial Y_n} \right] \\ c_n &= -\gamma \Delta t \frac{\partial F_n}{\partial Y_{n+1}} \\ d_n &= \Delta t \left\{ F_{n-1}^t - F_n^t - s_n^t \right\} \end{aligned} \quad (125)$$

The lefthandside of this equation represents the explicit update to the variable  $Y_n$  as in MOSES I. Note that no implicit correction is made to the sink term,  $s_n$ , since this would require an unwieldy implicit update to the entire coupled soil hydrology, soil thermodynamics and boundary layer system. By treating this term explicitly we decouple the updates to the soil temperatures and soil moistures, such that these variables can be incremented independently on each timestep. The equations represented by (124) are a tridiagonal set which can be solved routinely by Gaussian elimination (see appendix A for details).

The other major numerical difference between MOSES I and MOSES 2.2 involves the treatment of supersaturation in a soil layer. This can occur by two separate means. The first is a numerical artifact arising from the use of a finite timestep during which a very large quantity of incident water (for

example from a very intense rainstorm) can overflow the top soil layer. This occurred very infrequently in MOSES 1 (owing to the relatively thick top soil layer) and should be even less common within the implicit soil scheme of MOSES 2.2. Nevertheless, supersaturation can still occur when drainage from the base of a soil layer is impeded (either by frozen soil water or an assumed reduction of  $K_s$  with depth). Under these circumstances it may be necessary to return the soil water content in a layer to the saturation value. In MOSES 1 the excess water in a layer was arbitrarily routed downwards. The justification for this was weak, but based on the idea that such excess moisture might flow overland for some fraction of a large GCM gridbox, but would eventually move down through the soil profile at subgrid locations in which drainage is less impeded (e.g. where there is fractured permafrost or less compacted-faster draining soil types). However, this assumption was found to lead to poor runoff simulation and excessive soil moisture in the PILPS2d tests of MOSES 1 (?). In MOSES 2.2 excess moisture in a soil layer is instead removed by lateral flow which contributes to a larger fast runoff component. This alternative assumption is more consistent with the improved soil numerics (which should not lead to supersaturation as a numeric artifact), and results in much better water budgets for permafrost regions, such as the PILPS2d Valdai site.

## 5 Parameter aggregation

A single tile version of MOSES 2.2 can be selected by setting NTILES=1 in namelists RECON and NLSIZES. Separate surface parameters are still calculated for each surface type within a gridbox, but they are aggregated by routines SPARM, TILE\_ALBEDO and PHYSIOL before use. Albedos ( $\alpha_i$ ), maximum infiltration rate ( $\beta K_s$ ), canopy heat capacity ( $C_c$ ), canopy coverage ( $f_r$ ) and soil moisture extraction fractions ( $e_k$ ) are simply area-averaged. Canopy water capacity ( $C_m$ ) and surface conductance ( $g_s$ ) are averaged over the non-lake fractions of gridboxes. Roughness lengths are aggregated at a blending height  $l_b$  (set to 20 m in BLEND\_H.cdk) using the method of Mason (1988) to give

$$z_o = l_b \exp \left\{ - \left[ \sum_j \frac{v_j}{\ln^2(l_b/z_{oj})} \right]^{-1/2} \right\}. \quad (126)$$

# A Gaussian Elimination

The set of equations represented by (124) is solved by a two-sweep algorithm (subroutine GAUSS). Firstly, in an upward sweep, the  $\Delta Y_{n+1}$  terms are eliminated by transforming the  $n$ th equation,  $Eq(n)$ , thus:

$$Eq(n) \longrightarrow Eq(n)' = b'_{j+1} Eq(n) - c_n Eq(n+1)' \quad (127)$$

where  $'$  denotes a transformed equation or variable. Under this transformation the  $n$ th equation becomes:

$$a'_n \Delta Y_{n-1} + b'_n \Delta Y_n = d'_n \quad (128)$$

where:

$$\begin{aligned} a'_n &= b'_{n+1} a_n \\ b'_n &= b'_{n+1} b_n - a'_{n+1} c_n \\ d'_n &= b'_{n+1} d_n - d'_{n+1} c_n \end{aligned} \quad (129)$$

In the upward sweep  $a'_n$ ,  $b'_n$  and  $d'_n$  are evaluated iteratively beginning at the lowest soil layer, ( $N$ ), where the lower boundary conditions of the soil model imply  $c_N = 0$  such that  $a'_N = a_N$ ,  $b'_N = b_N$  and  $d'_N = d_N$ . In the downward sweep the increments to the prognostics variables,  $\Delta Y_n$  are derived iteratively from the top downwards using Equation (128):

$$\Delta Y_n = \frac{d'_n - a'_n \Delta Y_{n-1}}{b'_n} \quad (130)$$

The top boundary conditions of the soil model imply  $a_1 = 0$  such that  $\Delta Y_1 = d'_1/b'_1$ .

# B Array indexing

Routine TILEPTS sets array elements TILE\_PTS(J) to the number of gridboxes including surface type  $j$  and TILE\_INDEX(I, J) to the land array index of the  $i^{\text{th}}$  gridbox containing surface type  $j$ . Calculations for a specific surface type are only performed in gridboxes where that surface type is present. In UM version 4.5, loops of surface types and gridboxes take the form

```
DO N=1,NTILES
  DO J=1,TILE_PTS(N)
    L = TILE_INDEX(J,N)    ! Land field index
    I = LAND_INDEX(L)     ! Full field index
    .
    .
    .
  ENDDO
ENDDO
```

In version 5.2, two-dimensional indices are used for full field arrays :

```
DO N=1,NTILES
  DO K=1,TILE_PTS(N)
    L = TILE_INDEX(K,N)
    J = (LAND_INDEX(L)-1)/ROW_LENGTH + 1
    I = LAND_INDEX(L) - (J-1)*ROW_LENGTH
```

```
.  
. .  
ENDDO  
ENDDO
```

For use in NI\_rad\_ctl, the I and J indices are stored in arrays land\_index\_i and land\_index\_j.

# Description of the “TRIFFID” Dynamic Global Vegetation Model

Peter Cox

Hadley Centre, Met Office, London Road, Bracknell, Berks R12 2SY, UK  
*peter.cox@metoffice.com*

September 29, 2009

## Abstract

This note describes the terrestrial carbon cycle component of the Hadley Centre’s coupled climate-carbon cycle model (?). “TRIFFID (Top-down Representation of Interactive Foliage and Flora Including Dynamics)” is a dynamic global vegetation model, which updates the plant distribution and soil carbon based on climate-sensitive CO<sub>2</sub> fluxes at the land-atmosphere interface. The surface CO<sub>2</sub> fluxes associated with photosynthesis and plant respiration are calculated in the MOSES 2 tiled land-surface scheme (?), on each atmospheric model timestep (normally 30 minutes), for each of 5 plant functional types. The area covered by a plant type is updated (normally every 10 days) based on the net carbon available to it and on the competition with other plant types, which is modelled using a Lotka-Volterra approach. Soil carbon is increased by litterfall, which can arise from local processes such as leaf-drop as well as large-scale disturbances which reduce the vegetated area. Soil carbon is returned to the atmosphere by microbial respiration which occurs at a rate dependent on soil moisture and temperature. TRIFFID has been designed to allow economical diagnosis of initial states using a Newton-Raphson descent towards the equilibrium state consistent with a given climate.

## 1 Introduction

Over the last decade a number of groups have developed equilibrium biogeography models which successfully predict the global distribution of vegetation based on climate (?, ?). Such models have been coupled “asynchronously” to GCMs in order to quantify climate-vegetation feedbacks. This involves an iterative procedure in which the GCM calculates the climate implied by a given landcover, and the vegetation model calculates the landcover implied by a given climate. The process is repeated until a mutual climate-vegetation equilibrium is reached (?, ?). Such techniques have yielded very interesting results but suffer from two main limitations. Firstly, such asynchronous coupling may hide inconsistencies since the climate model and the vegetation model can represent common processes (such as the surface water balance) in different ways. This can lead to a mismatch between the variables and fluxes calculated in each. The second limitation is due to the implicit assumption that the climate and vegetation are in an equilibrium state. Although this may be a reasonable assumption for studying different vegetation-climate states on the timescales of interest in palaeoclimate modelling (?), it is not appropriate for simulating transient climate change over the next century, during which time the terrestrial biosphere is likely to be far from an equilibrium state.

In order to fully understand the role of climate-vegetation feedbacks on these timescales we need to treat the landcover as a interactive element, by incorporating dynamic global vegetation models (DGVMs) directly within climate models. The earliest DGVMs were based on bottom-up “gap” forest models, which explicitly model the growth, death and competition of individual plants (?, ?). Such models can produce very detailed predictions of vegetation responses to climate, but they are computationally expensive for large-scale applications. Also, GCM climates are not likely to be

sensitive to the details of the species or age composition of the landcover. For this study it is more appropriate to adopt a “top-down” DGVM approach, in which the relevant land-surface characteristics, such as vegetated fraction and leaf area index, are modelled directly (?). A model of this type, called “TRIFFID” (“Top-down Representation of Interactive Foliage and Flora Including Dynamics”), has been developed at the Hadley Centre for use in coupled climate-carbon cycle simulations (?).

## 2 Coupling to the GCM Land-Surface Scheme

TRIFFID defines the state of the terrestrial biosphere in terms of the soil carbon, and the structure and coverage of five plant functional types (Broadleaf tree, Needleleaf tree, C<sub>3</sub> grass, C<sub>4</sub> grass and shrub). The areal coverage, leaf area index and canopy height of each PFT are updated using a “carbon balance” approach, in which vegetation change is driven by net carbon fluxes calculated within the “MOSES 2” land surface scheme. MOSES 2 is a “tiled” version of the land surface scheme described by ?, in which a separate surface flux and temperature is calculated for each of the landcover types present in a GCM gridbox. In its standard configuration, MOSES 2 recognises the five TRIFFID vegetation types plus four non-vegetation landcover types (bare soil, inland water, urban areas and land ice). Carbon fluxes for each of the vegetation types are derived using the coupled photosynthesis-stomatal conductance model developed by ?, which utilises existing models of leaf-level photosynthesis in C<sub>3</sub> and C<sub>4</sub> plants (?, ?). Full details of this part of MOSES 2 are given in appendix ???. The resulting rates of photosynthesis and plant respiration are dependent on both climate and atmospheric CO<sub>2</sub> concentration. Therefore, with this carbon-balance approach, the response of vegetation to climate occurs via climate-induced changes in the vegetation to atmosphere fluxes of carbon.

Figure ?? is a schematic showing how the MOSES 2 land-surface scheme is coupled to TRIFFID for each vegetation type. The land-atmosphere fluxes (above the dotted line) are calculated within MOSES 2 on every 30 minute GCM timestep and time-averaged before being passed to TRIFFID (usually every 10 days). TRIFFID (below the dotted line of figure ??) allocates the average net primary productivity over this coupling period into the growth of the existing vegetation (leaf, root and wood biomass), and to the expansion of the “vegetated area”. Leaf phenology (bud-burst and leaf drop) is updated on an intermediate timescale of 1 day, using accumulated temperature-dependent leaf turnover rates. After each call to TRIFFID the land surface parameters required by MOSES 2 (e.g. albedo, roughness length) are updated based on the new vegetation state, so that changes in the biophysical properties of the land surface, as well as changes in terrestrial carbon, feedback onto the atmosphere (figure ??). The land surface parameters are calculated as a function of the type, height and leaf area index of the vegetation, as described in section ??.

Unlike the simplest asynchronous coupling techniques this structure ensures consistency between the surface hydrological states “seen” by the atmosphere and the vegetation. This is achieved by having a strong demarcation between the processes represented in TRIFFID and those represented in the MOSES 2 land-surface scheme. Specifically, MOSES 2 calculates instantaneous carbon fluxes (consistent with the modelled surface energy and water fluxes) using parameters provided by TRIFFID, whilst TRIFFID updates the vegetation and soil state (and associated parameters) using the accumulated fluxes passed from MOSES 2.

## 3 Vegetation Dynamics

At the core of TRIFFID are first order differential equations describing how the vegetation carbon density,  $C_v$ , and fractional coverage,  $\nu$ , of a given PFT are updated based on the carbon balance of that PFT and on competition with other PFTs:

$$\frac{dC_v}{dt} = (1 - \lambda) \Pi - \Lambda_l \tag{1}$$

$$C_v \frac{d\nu}{dt} = \lambda \Pi \nu_* \left\{ 1 - \sum_j c_{ij} \nu_j \right\} - \gamma \nu_* C_v \quad (2)$$

where  $\nu_* = \text{MAX} \{\nu, 0.01\}$ , and  $\Pi$  is the net primary productivity per unit vegetated area of the PFT in question (as calculated in the MOSES 2 land surface scheme). A fraction  $\lambda$  of this NPP is utilised in increasing the fractional coverage (equation ??), and the remainder increases the carbon content of the existing vegetated area (equation ??). Equation ?? therefore represents the local carbon balance as utilised in most terrestrial carbon cycle models. TRIFFID is unusual in that this is coupled to equation ??, which is based on the the Lotka-Volterra approach to intraspecies and interspecies competition (see for example ?). Lotka-Volterra equations are used frequently in theoretical population dynamics but have not previously been applied in a DGVM. In order to do so here, we have replaced the usual population state variable of number density with the fractional area covered by the PFT, and driven increases in  $\nu$  directly with NPP (via the first term on the righthandside of equation ??). Under most circumstances the variable  $\nu_*$  is identical to the areal fraction,  $\nu$ , but each PFT is “seeded” by ensuring that  $\nu_*$  never drops below the “seed fraction” of 0.01.

The competition coefficients,  $c_{ij}$ , represent the impact of vegetation type “j” on the vegetation type of interest (type “i”, although for clarity this subscript has been dropped from other variables in equations ?? and ??). These coefficients all lie between zero and unity, so that competition for space acts to reduce the growth of  $\nu$  that would otherwise occur (i.e. it produces density-dependent litter production). Each PFT experiences “intraspecies” competition, with  $c_{ii} = 1$  so that vegetation fraction is always limited to be less than one. Competition between natural PFTs is based on a tree-shrub-grass dominance heirarchy, with dominant types “i” limiting the expansion of subdominant types “j” ( $c_{ji} = 1$ ), but not vice-versa ( $c_{ij} = 0$ ). However, the tree types (broadleaf and needleleaf) and grass types ( $C_3$  and  $C_4$ ) co-compete with competition coefficients dependent on their relative heights,  $h_i$  and  $h_j$ :

$$c_{ij} = \frac{1}{1 + \exp \{20 (h_i - h_j)/(h_i + h_j)\}} \quad (3)$$

The form of this function ensures that the  $i^{\text{th}}$  PFT dominates when it is much taller, and the  $j^{\text{th}}$  PFT dominates in the opposite limit. The factor of 20 was chosen to give co-competition over a reasonable range of height differences. Some allowance is made for agricultural regions, from which the woody types (i.e. trees and grasses) are excluded, and  $C_3$  and  $C_4$  grasses are reinterpreted as “crops”.

The  $\lambda$  partitioning coefficient in equations ?? and ?? is assumed to be piecewise linear in the leaf area index, with all of the NPP being used for growth for small LAI values, and all the NPP being used for “spreading” for large LAI values:

$$\lambda = \begin{cases} 1 & \text{for } L_b > L_{max} \\ \frac{L_b - L_{min}}{L_{max} - L_{min}} & \text{for } L_{min} < L_b \leq L_{max} \\ 0 & \text{for } L_b \leq L_{min} \end{cases} \quad (4)$$

where  $L_{max}$  and  $L_{min}$  are parameters describing the maximum and minimum leaf area index values for the given plant functional type, and  $L_b$  is the “balanced” LAI which would be reached if the plant was in “full leaf”. The actual LAI depends on  $L_b$  and the phenological status of the vegetation type, which is updated as a function of temperature (see section ??).

Changes in vegetation carbon density,  $C_v$ , are related allometrically to changes in the balanced LAI,  $L_b$ . First,  $C_v$  is broken down into leaf,  $\mathcal{L}$ , root,  $\mathcal{R}$ , and total stem carbon,  $\mathcal{W}$ :

$$C_v = \mathcal{L} + \mathcal{R} + \mathcal{W} \quad (5)$$

Then each of these components are related to  $L_b$ . Root carbon is set equal to leaf carbon, which is itself linear in LAI, and total stem carbon is related to  $L_b$  by a power law (?):

$$\mathcal{L} = \sigma_l L_b \quad (6)$$

$$\mathcal{R} = \mathcal{L} \quad (7)$$

$$\mathcal{W} = a_{wl} L_b^{5/3} \quad (8)$$

Here  $\sigma_l$  is the specific leaf carbon density ( $\text{kg C m}^{-2} \text{LAI}^{-1}$ ) of the vegetation type, and  $a_{wl}$  is a PFT-dependent parameter in the power law relating LAI and total stem biomass. Recent work by ? suggests that 4/3 (rather than 5/3) may be a more appropriate power to use in the next version of TRIFFID. Values of canopy height,  $h$ , are directly from  $\mathcal{W}$  as described in section ??.

The local litterfall rate,  $\Lambda_l$ , in equation ??, consists of contributions from leaf, root and stem carbon:

$$\Lambda_l = \gamma_l \mathcal{L} + \gamma_r \mathcal{R} + \gamma_w \mathcal{W} \quad (9)$$

where  $\gamma_l$ ,  $\gamma_r$  and  $\gamma_w$  are turnover rates ( $\text{yr}^{-1}$ ) for leaf, root and stem carbon respectively. The leaf turnover rate is calculated to be consistent with the phenological module as described in section ??. The root turnover rate is set equal to the minimum leaf turnover rate  $\gamma_0 = 0.25$  for all PFTs, but the total stem turnover is PFT-dependent to reflect the different fractions of woody biomass (see table ??). There is an additional litter contribution arising from large-scale disturbance which results in loss of vegetated area at the prescribed rate  $\gamma_\nu$ , as represented by the last term on the righthandside of equation ??.

## 4 Leaf Phenology

Leaf mortality rates,  $\gamma_{lm}$ , for the tree-types are assumed to be a function of temperature, increasing from a minimum value of  $\gamma_0$ , as the leaf temperature drops below a threshold value,  $T_{off}$ :

$$\gamma_{lm} = \begin{cases} \gamma_0 & \text{for } T > T_{off} \\ \gamma_0 \{1 + 9(T_{off} - T)\} & \text{for } T \leq T_{off} \end{cases} \quad (10)$$

where  $T_{off} = 0^\circ\text{C}$  for broadleaf trees and  $T_{off} = -30^\circ\text{C}$  for needleleaf trees (?). The factor of 9 is such that the leaf turnover rate increases by a factor of 10 when the temperature drops  $1^\circ\text{C}$  below  $T_{off}$ . Equation ?? describes how leaf mortality varies with temperature, but it is not sufficient to produce realistic phenology. A new variable,  $p$ , is introduced which describes the phenological status of the vegetation:

$$L = p L_b \quad (11)$$

where  $L$  is the actual LAI of the canopy, and  $L_b$  is the balanced (or seasonal maximum) LAI as updated by TRIFFID via the inverse of equation ??. The phenological status,  $p$ , is updated on a daily basis assuming:

- leaves are dropped at a constant absolute rate ( $\gamma_p L_b$ ) when the daily mean value of leaf turnover, as given by equation ??, exceeds twice its minimum value
- budburst occurs at the same rate when  $\gamma_{lm}$  drops back below this threshold, and “full leaf” is approached asymptotically thereafter:

$$\frac{dp}{dt} = \begin{cases} -\gamma_p & \text{for } \gamma_{lm} > 2\gamma_0 \\ \gamma_p \{1 - p\} & \text{for } \gamma_{lm} \leq 2\gamma_0 \end{cases} \quad (12)$$

where  $\gamma_p = 20 \text{ yr}^{-1}$ . The effective leaf turnover rate,  $\gamma_l$ , as used in equation ??, must also be updated to ensure conservation of carbon when phenological changes are occurring:

$$\gamma_l = \begin{cases} -\frac{dp}{dt} & \text{for } \gamma_{lm} > 2\gamma_0 \\ p\gamma_{lm} & \text{for } \gamma_{lm} \leq 2\gamma_0 \end{cases} \quad (13)$$

Taken together, equation ??, ?? and ?? amount to a ‘‘chilling-days’’ parametrization of leaf phenology. A similar approach may be taken for drought-deciduous phenology and for the cold-deciduous phenology of the other (non-tree) PFTs, but neither is included in this version of TRIFFID.

## 5 Soil Carbon

Soil carbon storage,  $C_s$ , is increased by the total litterfall,  $\Lambda_c$ , and reduced by microbial soil respiration,  $R_s$ , which returns  $\text{CO}_2$  to the atmosphere:

$$\frac{dC_s}{dt} = \Lambda_c - R_s \quad (14)$$

In each gridbox, the total litterfall is made-up of the area-weighted sum of the local litterfall from each PFT (as given by equation ??), along with terms due to the large-scale disturbance rate,  $\gamma_\nu$ , and PFT competition:

$$\Lambda_c = \sum_i \nu_i \left\{ \Lambda_{li} + \gamma_{\nu i} C_{vi} + \Pi_i \sum_j c_{ij} \nu_j \right\} \quad (15)$$

The competition term (last term on the righthand side of equation ??) is derived by imposing carbon conservation on the soil-vegetation system as described by equations ??, ?? and ??. It implies that the NPP of each PFT will be lost entirely as litter once the PFT occupies all of the space available to it (i.e. when  $\sum_j c_{ij} \nu_j = 1$ ).

The rate of soil respiration,  $R_s$ , is dependent on the soil temperature,  $T_s$ , volumetric soil moisture concentration,  $\Theta$ , and soil carbon content,  $C_s$ :

$$R_s = \kappa_s C_s f_\Theta f_T \quad (16)$$

where  $\kappa_s = 5 \times 10^{-9} \text{ s}^{-1}$  is the specific soil respiration rate at  $25^\circ \text{C}$ , and  $f_\Theta$  and  $f_T$  are moisture and temperature dependent functions respectively. The latter is assumed to take the ‘‘Q10’’ form:

$$f_T = q_{10}^{0.1(T_s - 25)} \quad (17)$$

where  $T_s$  is the soil temperature in  $^\circ\text{C}$  and  $q_{10} = 2.0$ . The moisture dependence is based on the model of ? in which the respiration rate increases with soil moisture content until an optimum value of moisture is reached. Thereafter the rate of respiration is reduced with further increases in soil moisture. The curves presented by ? were approximated by piecewise linear functions in order to minimise the number of additional soil variables required.

$$f_\Theta = \begin{cases} 1 - 0.8 \{S - S_o\} & \text{for } S > S_o \\ 0.2 + 0.8 \left\{ \frac{S - S_w}{S_o - S_w} \right\} & \text{for } S_w < S \leq S_o \\ 0.2 & \text{for } S \leq S_w \end{cases} \quad (18)$$

Here  $S$ ,  $S_w$  and  $S_o$  are the (unfrozen) soil moisture, the wilting soil moisture and the optimum soil moisture as a fraction of saturation:

$$S = \frac{\Theta}{\Theta_s} \quad (19)$$

$$S_w = \frac{\Theta_w}{\Theta_s} \quad (20)$$

$$S_o = 0.5 \{1 + S_w\} \quad (21)$$

where  $\Theta$ ,  $\Theta_s$  and  $\Theta_w$  are the (unfrozen) soil moisture concentration, the saturation soil moisture concentration and the wilting soil moisture concentration respectively.

## 6 Updating Biophysical Parameters

In order to close the biophysical feedback loop (see figure ??), the land-surface parameters required by the MOSES 2 land-surface scheme (?) are recalculated directly from the LAI and canopy height of each PFT, each time the vegetation cover is updated. Values of canopy height,  $h$ , are derived by assuming a fixed ratio,  $a_{ws}$ , of total stem carbon,  $\mathcal{W}$ , to respiring stem carbon,  $\mathcal{S}$ :

$$\mathcal{W} = a_{ws} \mathcal{S} \quad (22)$$

where we assume  $a_{ws} = 10.0$  for woody plants and  $a_{ws} = 1.0$  for grasses (?). Combining with equations ?? and ?? enables canopy height to be diagnosed directly from the total stem biomass:

$$h = \frac{\mathcal{W}}{a_{ws} \eta_{sl}} \left\{ \frac{a_{wl}}{\mathcal{W}} \right\}^{1/b_{wl}} \quad (23)$$

The aerodynamic roughness lengths, which are used by MOSES 2 to calculate surface-atmosphere fluxes of heat, water, momentum and  $\text{CO}_2$ , are assumed to be directly proportional to this canopy height:

$$z_0 = \begin{cases} 0.05 h & \text{for trees} \\ 0.10 h & \text{for grasses and shrubs} \end{cases} \quad (24)$$

where  $z_0$  is the roughness length for momentum. The roughness lengths for scalars (heat, water and  $\text{CO}_2$ ) are taken to be 0.1 of this value.

The snow-free albedo of each vegetation tile,  $\alpha_0$ , is calculated as a weighted sum of the soil albedo,  $\alpha_{00}$ , and a prescribed maximum canopy albedo,  $\alpha_{0\infty}$ :

$$\alpha_0 = \alpha_{00} \exp\{-kL\} + \alpha_{0\infty} (1 - \exp\{-kL\}) \quad (25)$$

where  $L$  is the LAI,  $k = 0.5$  and  $\exp\{-kL\}$  represents the fraction of the incident light which passes through to the soil surface. This simple albedo parametrization uses values of  $\alpha_{0\infty} = 0.1$  for tree types, and  $\alpha_{0\infty} = 0.2$  for grasses and shrubs. The soil albedo is a geographically varying field derived from the dataset of ?. A similar equation is used to calculate the ‘‘cold deep-snow’’ albedo, but here both albedo parameters are PFT-dependent. We assume maximum snow albedos of  $\alpha_{s0} = 0.3$  for trees, and  $\alpha_{s0} = 0.8$  for shrubs and grasses. The prescribed minimum snow albedos are;  $\alpha_{s\infty} = 0.15$  for the tree types,  $\alpha_{s\infty} = 0.6$  for grass types and  $\alpha_{s\infty} = 0.4$  for shrubs. In all cases these parameters were chosen to approximate the albedo values used by ?.

The canopy catchment capacity,  $c_m$ , which determines the amount of water which is freely available for evaporation from the surface, varies linearly with LAI:

$$c_m = 0.5 + 0.05 L \quad (26)$$

where the offset of 0.5 represents puddling of water on the soil surface and interception by leafless plants. The other hydrological land-surface parameters required by MOSES 2 are PFT-dependent,

but do not depend directly on LAI or canopy height in this version. Root density is taken to fall off exponentially with depth, such that it is  $e^{-2}$  of its surface value at a specified rootdepth (of 3.0m for broadleaf trees, 1.0m for needleleaf trees and 0.5m for grasses and shrubs). Roots are assumed to enhance the maximum surface infiltration rate for water by a factor of 4 for trees, and 2 for the other PFTs.

## 7 Spin-up Methodology

Soil carbon and forest area have timescales of order 1000 years to reach equilibrium which means it is not feasible to carry out this spin-up in the fully coupled GCM. However, it is still vital to reach a good approximation to the pre-industrial equilibrium. The contemporary carbon sink is only a small fraction of the gross carbon exchanges between the Earth’s surface and the atmosphere, and any significant model drift could easily swamp this signal. With this in mind, TRIFFID was designed to be usable in both “equilibrium” and “dynamic” mode.

This flexibility relies on the numerical design of the model. The TRIFFID equations to update the plant fractional coverage and leaf area index are written to enable both “explicit” and “implicit” timestepping. Thus for example, the dynamical equation for leaf area index,  $L$ , can be represented by:

$$\frac{dL}{dt} = F(L) \quad (27)$$

where  $F$  is a non-linear function of  $L$ . An explicit scheme uses the beginning-of-timestep value,  $L_n$ , to calculate  $F$ , whilst a fully implicit scheme uses the end-of-timestep value,  $L_{n+1}$ . In general the update equation may be written:

$$\frac{\Delta L}{\Delta t} = F(L_n + f\Delta L) \quad (28)$$

where  $\Delta t$  is the model timestep and  $f$  is the “forward timestep weighting factor”, which is 0 for an explicit scheme and 1 for a fully implicit scheme. Taylor expansion about  $L_n$  provides an algebraic update for  $L$ :

$$\Delta L = \frac{F(L_n) \Delta t}{1 - f F'(L_n) \Delta t} \quad (29)$$

where  $F'(L_n)$  is the derivative of  $F$  with respect to  $L$  at  $L = L_n$ . For  $f = 1$  and large timesteps this equation reduces to the Newton-Raphson algorithm for iteratively approaching the equilibrium given by  $F(L) = 0$ .

Each of the TRIFFID prognostic equations is written in the form represented by equation ??, which allows the model to be used in two distinct modes. In “equilibrium mode” TRIFFID is coupled asynchronously to the atmospheric model, with accumulated carbon fluxes passed from MOSES 2 typically every 5 or 10 years. On each TRIFFID call, the vegetation and soil variables are updated iteratively using an implicit scheme ( $f = 1$ ) with a long internal timestep (10,000 years by default). Offline tests have shown that this approach is very effective in producing equilibrium states for the slowest variables (e.g. soil carbon and forest cover). In “dynamic mode”, equation ?? is used with  $f = 0$  and a timestep equal to the TRIFFID-GCM coupling period (typically 10 days).

Although the equilibrium mode is effective at bringing the slower components to equilibrium, it is often necessary to carry-out a subsequent dynamical TRIFFID run so as to allow the faster varying components (such as grasses) to come into equilibrium with the seasonally varying climate. During the pre-industrial spin-up of the HadCM3LC coupled climate-carbon cycle model (?) we completed a 60 year GCM run with TRIFFID in equilibrium mode (5 year coupling period) and followed this by a GCM simulation of 90 years with TRIFFID in its dynamical mode (10 day coupling period). This was necessary to meet the rather stringent requirements of net carbon balance set to ensure that the current carbon sink was not swamped by model drift. For many other purposes (such as simulations of palaeoclimate-vegetation interactions) much shorter simulations should suffice (e.g. 20 years in equilibrium mode followed by 10 years in dynamical mode).

## 8 Further Reading

We have described the TRIFFID dynamic global vegetation model which has been coupled consistently to the Met Office/Hadley Centre GCM. TRIFFID has already been successfully used in coupled climate-carbon cycle simulations, where it reproduces the key features of the global vegetation distribution (?) and contributes to realistic variability in the global carbon cycle (?, ?). Scenarios of future climate change computed with the coupled climate-carbon cycle model suggest that land carbon cycle feedbacks (from TRIFFID) could significantly accelerate global warming in the next century (?). Copies of these papers and reports can be obtained on request from the author.

# A Vegetation Carbon Fluxes

## A.1 Basic Model Structure

Stomatal openings are the pathways through which both water and carbon dioxide are exchanged between vegetation and the atmosphere. Consequently, net leaf photosynthesis,  $A$  (mol CO<sub>2</sub> m<sup>-2</sup> s<sup>-1</sup>), and stomatal conductance to water vapour,  $g_s$  (m s<sup>-1</sup>), are linked through:

$$A = \frac{g_s}{1.6 R T_*} (c_c - c_i) \quad (30)$$

where  $R$  is the perfect gas constant,  $T_*$  (K) is the leaf surface temperature, and  $c_c$  and  $c_i$  (Pa) are the leaf surface and internal CO<sub>2</sub> partial pressures respectively. The factor of 1.6 accounts for the different molecular diffusivities of water and carbon dioxide. Leaf photosynthesis is known to be dependent on a number of environmental variables as well as the internal CO<sub>2</sub> concentration,  $c_i$ :

$$A = A(\vec{X}, c_i) \quad (31)$$

where  $\vec{X}$  represents a general vector of environmental variables. Equations ?? and ?? contain three unknowns;  $A$ ,  $g$  and  $c_i$ . The closure suggested by ? is in MOSES (?, ?):

$$\left\{ \frac{c_i - \Gamma}{c_c - \Gamma} \right\} = F_0 \left\{ 1 - \frac{D_*}{D_c} \right\} \quad (32)$$

where  $\Gamma$  is the internal partial pressure of CO<sub>2</sub> at which photosynthesis just balances photorespiration (the “photorespiration compensation point”),  $D_*$  is the humidity deficit at the leaf surface, and  $F_0$  and  $D_c$  are vegetation specific parameters (see table ??). The leaf photosynthesis models represented by ?? are based on the work of ? and ? for C<sub>3</sub> and C<sub>4</sub> plants respectively. Details of these models are given below. However, an additional direct soil moisture dependence is introduced as suggested by ?:

$$A = A_p \beta \quad (33)$$

where  $A_p$  is the “potential” (non-moisture stressed) rate of net photosynthesis as given by the models described below, and  $\beta$  is the moisture stress factor:

$$\beta = \begin{cases} 1 & \text{for } \Theta > \Theta_c \\ \frac{\Theta - \Theta_w}{\Theta_c - \Theta_w} & \text{for } \Theta_w < \Theta \leq \Theta_c \\ 0 & \text{for } \Theta \leq \Theta_w \end{cases} \quad (34)$$

Here,  $\Theta_c$  and  $\Theta_w$  are the critical and wilting soil moisture concentrations respectively, and  $\Theta$  is the mean soil moisture concentration in the rootzone.

Equations ?? to ?? represent a coupled model of stomatal conductance and leaf photosynthesis. Large-scale applications require an economical means of scaling the predicted leaf-level fluxes up to the canopy scale. The approach of ? is used here, in which the primary determinants of photosynthesis, mean incident photosynthetically active radiation (PAR),  $I_{par}$ , and the maximum rate of carboxylation of Rubisco,  $V_{max}$ , are assumed to be proportional throughout the plant canopy:

$$I_{par}(l) = I_{par}(0) \exp \{-k l\} \quad (35)$$

$$V_{max}(l) = V_{max}(0) \exp \{-k l\} \quad (36)$$

where  $(l)$  denotes values beneath  $l$  leaf layers,  $(0)$  denotes values at the top of the canopy, and  $k = 0.5$  is the PAR extinction coefficient. This assumption ensures that the relative importance of each of the photosynthesis limiting factors is the same at every depth in the canopy. As a consequence it is straightforward to integrate the leaf conductance and photosynthesis over the canopy leaf area index,

$L$ , to yield canopy conductance,  $g_c$ , net canopy photosynthesis,  $A_c$ , and (non-moisture stressed) canopy dark respiration,  $R_{dc}$ :

$$g_c = g f_{par} \quad (37)$$

$$A_c = A f_{par} \quad (38)$$

$$R_{dc} = R_d f_{par} \quad (39)$$

where  $g$ ,  $A$  and  $R_d$  are the conductance, net photosynthesis and (non-moisture stressed) dark respiration rate of the top leaf layer and

$$f_{par} = \frac{1 - \exp\{-kL\}}{k} \quad (40)$$

Gross primary productivity,  $\Pi_G$ , is equivalent to the gross canopy photosynthesis:

$$\Pi_G = 0.012 \{A_c + R_{dc} \beta\} \quad (41)$$

where the factor 0.012 converts from units of ( $\text{mol CO}_2 \text{ m}^{-2} \text{ s}^{-1}$ ) to ( $\text{kg C m}^{-2} \text{ s}^{-1}$ ), and the second term in the brackets is the actual (moisture modified) canopy dark respiration. Net primary productivity,  $\Pi$  ( $\text{kg C m}^{-2} \text{ s}^{-1}$ ), is:

$$\Pi = \Pi_G - R_p \quad (42)$$

where  $R_p$  ( $\text{kg C m}^{-2} \text{ s}^{-1}$ ) is the total plant respiration. The calculation of  $R_p$  is described in subsection ??.

## A.2 Leaf Photosynthesis Models

The  $C_3$  and  $C_4$  photosynthesis models are based on the work of ? and ?, as applied by ?. In both cases the rate of gross leaf photosynthesis,  $W$  ( $\text{mol CO}_2 \text{ m}^{-2} \text{ s}^{-1}$ ), is calculated in terms of three potentially limiting factors:

- (i)  $W_c$  represents the rate of gross photosynthesis when the photosynthetic enzyme system (RuBP) is limiting:

$$W_c = \begin{cases} V_m \left\{ \frac{c_i - \Gamma}{c_i + K_c (1 + O_a/K_o)} \right\} & \text{for } C_3 \text{ plants} \\ V_m & \text{for } C_4 \text{ plants} \end{cases} \quad (43)$$

where  $V_m$  ( $\text{mol CO}_2 \text{ m}^{-2} \text{ s}^{-1}$ ) is the maximum rate of carboxylation of Rubisco,  $O_a$  (Pa) is the partial pressure of atmospheric oxygen, and  $K_c$  and  $K_o$  (Pa) are Michaelis-Menten constants for  $\text{CO}_2$  and  $\text{O}_2$  respectively.

- (ii)  $W_l$  is the light-limited rate of gross photosynthesis:

$$W_l = \begin{cases} 0.08 (1 - \omega) I_{par} \left\{ \frac{c_i - \Gamma}{c_i + 2\Gamma} \right\} & \text{for } C_3 \text{ plants} \\ 0.04 (1 - \omega) I_{par} & \text{for } C_4 \text{ plants} \end{cases} \quad (44)$$

where  $I_{par}$  is the incident photosynthetically active radiation ( $\text{mol PAR photons m}^{-2} \text{ s}^{-1}$ ) and  $\omega$  is the leaf scattering coefficient for PAR. The coefficients of 0.08 and 0.04 represent the ‘‘quantum efficiency’’ of  $C_3$  and  $C_4$  plants respectively. We follow ? and ? in assuming  $\omega = 0.15$  for  $C_3$  plants, and  $\omega = 0.17$  for  $C_4$  plants.

- (iii)  $W_e$  is the limitation associated with transport of the photosynthetic products for C<sub>3</sub> plants, but is the PEP-Carboxylase limitation for C<sub>4</sub> plants (?):

$$W_e = \begin{cases} 0.5 V_m & \text{for C}_3 \text{ plants} \\ 2 \times 10^4 V_m \frac{c_i}{p_*} & \text{for C}_4 \text{ plants} \end{cases} \quad (45)$$

where  $p_*$  is the surface air pressure.

The actual rate of gross photosynthesis,  $W$ , is calculated as the smoothed minimum of these three limiting rates:

$$\beta_1 W_p^2 - W_p \{W_c + W_l\} + W_c W_l = 0 \quad (46)$$

$$\beta_2 W^2 - W \{W_p + W_e\} + W_p W_e = 0 \quad (47)$$

where  $W_p$  is the smoothed minimum of  $W_c$  and  $W_l$ , and  $\beta_1 = 0.83$  and  $\beta_2 = 0.93$  are ‘‘co-limitation’’ coefficients. The smallest root of each quadratic is selected. Finally (non-moisture stressed) net leaf photosynthesis,  $A_p$ , is calculated by subtracting the rate of dark respiration,  $R_d$ , from the gross photosynthetic rate,  $W$ :

$$A_p = W - R_d \quad (48)$$

The parameters  $R_d$ ,  $V_m$ ,  $K_o$ ,  $K_c$  and  $\Gamma$  are all temperature dependent functions derived from ? for C<sub>3</sub> plants and ? for C<sub>4</sub> plants:

- $V_m$ , (mol CO<sub>2</sub> m<sup>-2</sup> s<sup>-1</sup>) the maximum rate of carboxylation of Rubisco:

$$V_m = \frac{V_{max} f_T(2.0)}{[1 + \exp \{0.3 (T_c - T_{upp})\}] [1 + \exp \{0.3 (T_{low} - T_c)\}]} \quad (49)$$

where  $T_c$  is the leaf temperature in °C,  $T_{upp}$  and  $T_{low}$  are PFT-dependent parameters, and  $f_T$  is the standard ‘‘Q10’’ temperature dependence:

$$f_T(q_{10}) = q_{10}^{0.1(T_c - 25)} \quad (50)$$

The standard photosynthesis models of ? and ? assume specific values of  $T_{upp}$  and  $T_{low}$  for C<sub>3</sub> and C<sub>4</sub> plants respectively ( $T_{low} \rightarrow -\infty$ ,  $T_{upp} = 36$  °C for C<sub>3</sub> plants, and  $T_{low} = 13$  °C,  $T_{upp} = 45$  °C for C<sub>4</sub> plants). However, in order to capture the temperature responses of all terrestrial ecosystems, it is necessary to make these parameters more generally dependent on PFT (i.e. not just dependent on the photosynthetic pathway). Values of the values chosen are shown in table ??.

$V_{max}$  (mol CO<sub>2</sub> m<sup>-2</sup> s<sup>-1</sup>) is assumed to be linearly dependent on the leaf nitrogen concentration,  $n_l$  (kg N (kg C)<sup>-1</sup>):

$$V_{max} = \begin{cases} 0.0008 n_l & \text{for C}_3 \text{ plants} \\ 0.0004 n_l & \text{for C}_4 \text{ plants} \end{cases} \quad (51)$$

The constants of proportionality are derived from ? by assuming that dry matter is 40 % carbon by mass and that the maximum rate of photosynthesis is approximately equal to  $0.5V_{max}$  for C<sub>3</sub> plants and approximately equal to  $V_{max}$  for C<sub>4</sub> plants.

- $\Gamma$ , (Pa) the photorespiration compensation point:

$$\Gamma = \begin{cases} \frac{O_a}{2\tau} & \text{for C}_3 \text{ plants} \\ 0 & \text{for C}_4 \text{ plants} \end{cases} \quad (52)$$

where  $\tau$  is the Rubisco specificity for CO<sub>2</sub> relative to O<sub>2</sub>:

$$\tau = 2600 f_T(0.57) \quad (53)$$

- $K_c$  and  $K_o$  (Pa), Michaelis-Menten constants for  $\text{CO}_2$  and  $\text{O}_2$ :

$$K_c = 30 f_T(2.1) \quad (54)$$

$$K_o = 3 \times 10^4 f_T(1.2) \quad (55)$$

- The rate of dark respiration,  $R_d$  ( $\text{mol CO}_2 \text{ m}^{-2} \text{ s}^{-1}$ ) is also assumed to have a “Q10” temperature dependence, with a constant of proportionality which depends on  $V_{max}$  (i.e. leaf nitrogen concentration):

$$R_d = \begin{cases} 0.015 V_{max} f_T(2.0) & \text{for C}_3 \text{ plants} \\ 0.025 V_{max} f_T(2.0) & \text{for C}_4 \text{ plants} \end{cases} \quad (56)$$

Note: this differs from the dark respiration rate used by ? and ?, which was taken to be directly proportional to  $V_m$  as given by ??.

### A.3 Plant Respiration

Plant respiration,  $R_p$ , is split into maintenance and growth respiration:

$$R_p = R_{pm} + R_{pg} \quad (57)$$

Growth respiration is assumed to be a fixed fraction of the net primary productivity, thus:

$$R_{pg} = r_g \{ \Pi_G - R_{pm} \} \quad (58)$$

where  $\Pi_G$  is the gross primary productivity, and the growth respiration coefficient is set to  $r_g = 0.25$  for all plant functional types. Leaf maintenance respiration is equivalent to the moisture modified canopy dark respiration,  $\beta R_{dc}$ , while root and stem respiration is assumed to be independent of soil moisture, but to have the same dependences on nitrogen content and temperature. Thus total maintenance respiration is given by:

$$R_{pm} = 0.012 R_{dc} \left\{ \beta + \frac{(N_r + N_s)}{N_l} \right\} \quad (59)$$

where  $N_l$ ,  $N_s$  and  $N_r$  are the nitrogen contents of leaf, stem and root, and the factor of 0.012 converts from ( $\text{mol CO}_2 \text{ m}^{-2} \text{ s}^{-1}$ ) to ( $\text{kg C m}^{-2} \text{ s}^{-1}$ ). The nitrogen contents are given by:

$$N_l = n_l \sigma_l L \quad (60)$$

$$N_r = \mu_{rl} n_l \mathcal{R} \quad (61)$$

$$N_s = \mu_{sl} n_l \mathcal{S} \quad (62)$$

where  $n_l$  is the mean leaf nitrogen concentration ( $\text{kg N (kg C)}^{-1}$ ),  $\mathcal{R}$  and  $\mathcal{S}$  are the carbon contents of respiring root and stem,  $L$  is the canopy leaf area index and  $\sigma_l$  ( $\text{kg C m}^{-2}$ ) is the specific leaf density. The nitrogen concentrations of root and stem are assumed to be fixed (functional type dependent) multiples,  $\mu_{rl}$  and  $\mu_{sl}$ , of the mean leaf nitrogen concentration. In this study, we assume  $\mu_{rl} = 1.0$  for all PFTS,  $\mu_{sl} = 0.1$  for woody plants (trees and shrubs) and  $\mu_{sl} = 1.0$  for grasses. The respiring stemwood is calculated using a “pipemodel” approach in which live stemwood is proportional to leaf area,  $L$ , and canopy height,  $h$ :

$$\mathcal{S} = 0.01 h L \quad (63)$$

The constant of proportionality is approximated from ?.

Parameter	Units	Broadleaf Tree	Needleleaf Tree	C <sub>3</sub> Grass	C <sub>4</sub> Grass	Shrub
$a_{wl}$	kg C m <sup>-2</sup>	0.650	0.650	0.005	0.005	0.100
$\gamma_\nu$	yr <sup>-1</sup>	0.004	0.004	0.100	0.100	0.030
$\gamma_w$	yr <sup>-1</sup>	0.010	0.010	0.200	0.200	0.050
$\gamma_0$	yr <sup>-1</sup>	0.250	0.250	0.250	0.250	0.250
$L_{max}$		9	9	4	4	4
$L_{min}$		3	3	1	1	1

Table 1: PFT-specific parameters for the dynamic vegetation component of TRIFFID. The values of  $a_{wl}$  were chosen to give realistic maximum biomass densities from equation ???. The other parameters were chosen largely by model calibration in offline tests, but realistic constraints were applied. For example, the large-scale disturbance rate,  $\gamma_\nu$ , should yield realistic effective plant lifetimes, and the total stemwood turnover rate,  $\gamma_w$ , should reflect the differing percentages of wood amongst the PFTs. The minimum leaf turnover rate,  $\gamma_0$ , was set uniform across the PFTs for simplicity. This value is also used to specify the turnover of root biomass.

Parameter	Units	Broadleaf Tree	Needleleaf Tree	C <sub>3</sub> Grass	C <sub>4</sub> Grass	Shrub
$n_l(0)$	kg N (kg C) <sup>-1</sup>	0.040	0.030	0.060	0.030	0.030
$\sigma_l$	kg C m <sup>-2</sup> LAI <sup>-1</sup>	0.0375	0.100	0.025	0.050	0.050
$F_0$		0.875	0.875	0.900	0.800	0.900
$D_c$	kg (kg) <sup>-1</sup>	0.090	0.060	0.100	0.075	0.100
$T_{low}$	°C	0	-5	0	13	0
$T_{upp}$	°C	36	31	36	45	36

Table 2: PFT-specific parameters used in the MOSES 2 calculation of vegetation carbon fluxes. The values for top-leaf nitrogen concentration,  $n_l(0)$ , and specific leaf density,  $\sigma_l$ , are derived from the survey of Schulze *et al* (1994), which suggests that  $n_l(0) \sigma_l = 1.5 \times 10^{-3}$  kg N m<sup>-2</sup> LAI<sup>-1</sup> for broadleaf plants, and  $n_l(0) \sigma_l = 3 \times 10^{-3}$  kg N m<sup>-2</sup> LAI<sup>-1</sup> for needleleaf plants. Values of the maximum ratio of internal to external CO<sub>2</sub>,  $F_0$ , and the critical humidity deficit,  $D_c$ , are chosen to give realistic maxima and humidity dependences for the canopy conductance (see for example, Cox *et al* (1998)). The lower and upper temperatures for photosynthesis,  $T_{low}$  and  $T_{upp}$  are consistent with the values prescribed by Collatz *et al* (1991) and Collatz *et al* (1992), except for the introduction of a finite lower bound for the C<sub>3</sub> plants, and the shift of the  $V_m$  curve for needleleaf trees by -5°C.

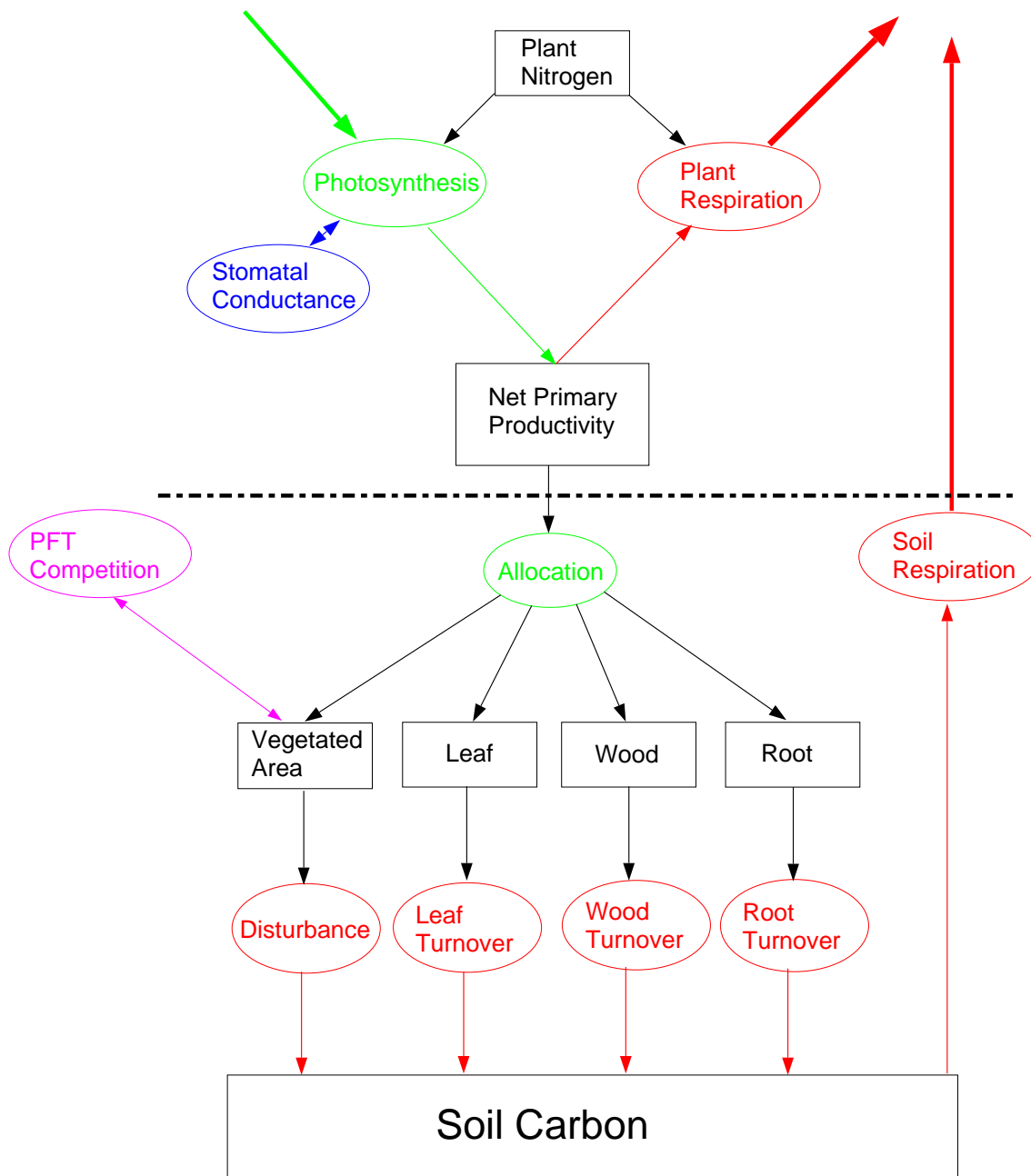


Figure 1: Schematic showing TRIFFID carbon flows for each vegetation type. Processes above the dotted line are fluxes calculated in the MOSES 2 land surface scheme every atmospheric model timestep ( $\approx 30$  minutes). In dynamic mode, TRIFFID updates the vegetation and soil carbon every 10 days using time-averages of these fluxes.

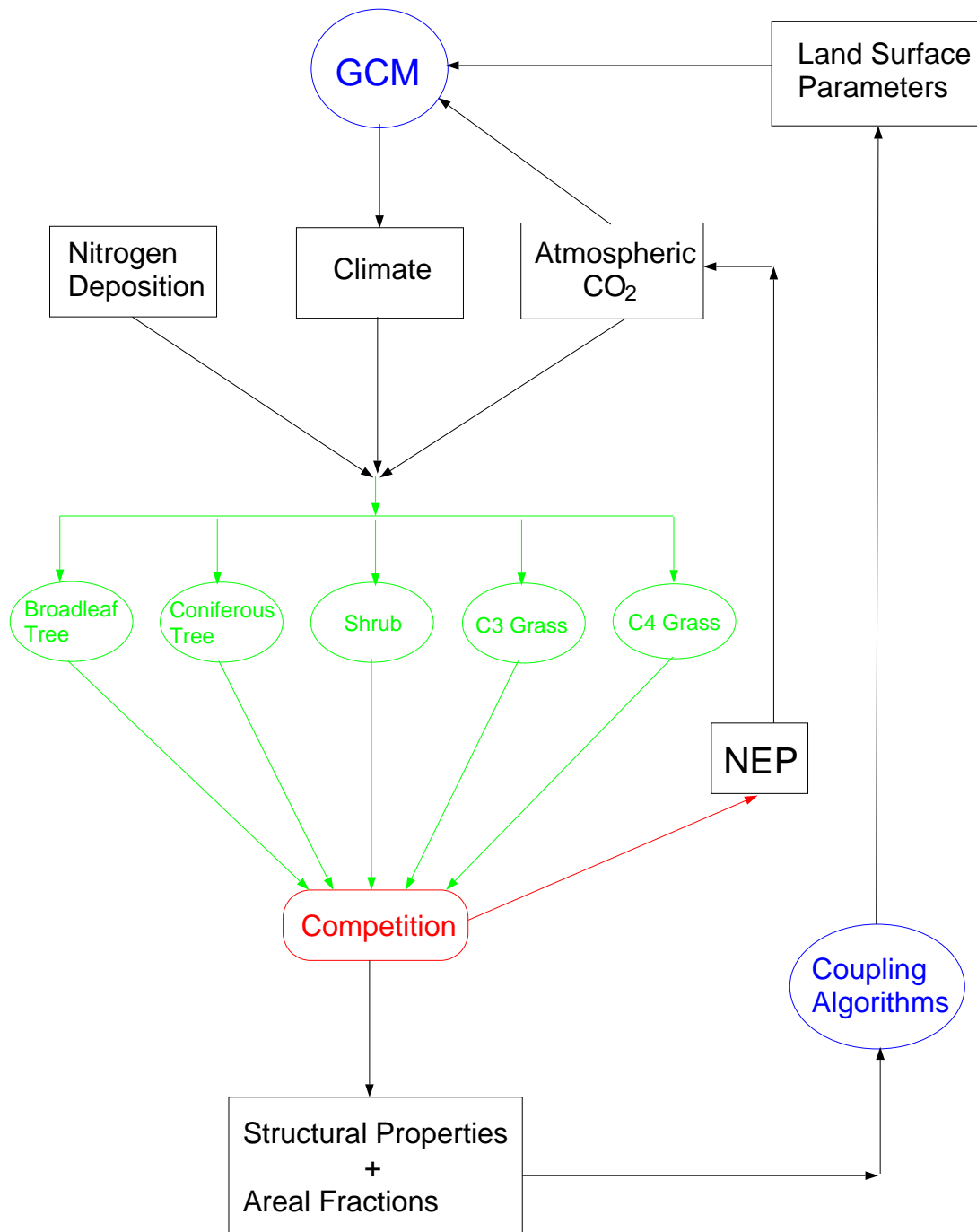


Figure 2: Schematic showing the coupling between TRIFFID and the GCM. Changes in the distribution and structure of the five plant functional types can provide a feedback to climate via two routes. The vegetation determines the biophysical land-surface parameters (e.g. albedo, roughness length, stomatal conductance) which in turn affect the land-atmosphere fluxes of heat, water and momentum. In addition, changes in the carbon stored in vegetation and soil (as measured by the net ecosystem productivity, “NEP”) can change the evolution of atmospheric CO<sub>2</sub> and thus the climate through the greenhouse effect. For completeness nitrogen deposition is also shown as a driver for vegetation change, although this version of TRIFFID does not include an interactive nitrogen cycle.